N O T I C E

THIS DOCUMENT HAS BEEN REPRODUCED FROM MICROFICHE. ALTHOUGH IT IS RECOGNIZED THAT CERTAIN PORTIONS ARE ILLEGIBLE, IT IS BEING RELEASED IN THE INTEREST OF MAKING AVAILABLE AS MUCH INFORMATION AS POSSIBLE

JPL PUBLICATION 81-100

(JPL-Pub-81-100) EXPERIMENTAL AND ANALYTICAL INVESTIGATION OF A FLUIDIC POWER GENERATOR (Jet Propulsion Lab.) 81 p
A05/MF A01 CSCL 20D

N82-13386

Unclas
G3/34 08457

Experimental and Analytical Investigation of a Fluidic Power Generator

V. Sarohia
L. Bernal
R. B. Beauchamp

November 15, 1981

Prepared for
Harry Diamond Laboratories,
U. S. Department of the Army
Through an agreement with
National Aeronautics and Space Administration
by
Jet Propulsion Laboratory
California Institute of Technology
Pasadena, California

JPL PUBLICATION 81-100

Experimental and Analytical Investigation of a Fluidic Power Generator

V. Sarohia
L. Bernal
R. B. Beauchamp

November 15, 1981

Prepared for
Harry Diamond Laboratories,
U. S. Department of the Army
Through an agreement with
National Aeronautics and Space Administration
by
Jet Propulsion Laboratory
California Institute of Technology
Pasadena, California

The research described in this publication was carried out by the Jet Propulsion Laboratory, California Institute of Technology, and was sponsored by the U.S. Department of the Army under an agreement with the National Aeronautics and Space Administration.

CONTENTS

LIST OF APPENDIXES

LIST OF TABLES

LIST OF FIGURES

NOMENCLATURE

A	area
a	speed of sound
B	jet layer parameter
C_v	mass flow coefficient
d	diameter
$F(\zeta)$	function describing resonant properties of the generator
$f(M)$	function describing acoustical properties of nozzle
f	frequency
f_D	diaphragm-reed friction coefficient
g_o	acceleration of gravity, sea-level value
H	geopotential altitude
h_o	ram-air jet width
I	flow inertia parameter
i	$= \sqrt{-1}$
K	non-dimensional cavity volume
k_D	diaphragm-reed spring constant
ℓ	distance from ram-air jet to tube
L	tube length
$M( )$	function describing resonant characteristics of the tube
M_o	molecular weight of air
M_1	generator flight Mach number
m_D	diaphragm-reed effective mass
$\dot{m}$	mass flow
p	pressure
q	ram-air jet velocity
R	reflection coefficient

Nomenclature, (Continued)

R^*	universal gas constant
R_J	radius of curvature, jet layer
R_e	$= \frac{\dot{m}d}{A\mu}$, Reynolds number
r_o	effective earth radius
T	temperature
t	time
U	velocity
V	volume
v	velocity component across the flow direction
W	jet layer perimeter
x	downstream distance
x_D	diaphragm-reed position
Z	geometrical altitude
z	$= (\sigma+i\omega)$ complex frequency
α,β	non-dimensional parameters
γ	specific heat ratio
ζ	non-dimensional complex frequency
η	diaphragm-reed non-dimensional parameter
μ	viscosity
μ_J	$= \frac{\hat{\dot{m}}_J}{\hat{\dot{m}}_T}$
μ_H	$= \frac{\hat{\dot{m}}_H}{\hat{\dot{m}}_T}$
σ	real part complex frequency
σ_T	$= \frac{\hat{p}_T}{\hat{\dot{m}}_T} \frac{A_T}{a}$
σ_C	$= \frac{\hat{p}_C}{\hat{\dot{m}}_T} \frac{A_T}{a}$

ϕ,Ω	diaphragm-reed non-dimensional parameters
ω	imaginary part complex frequency

SUBSCRIPTS AND SUPERSCRIPTS

$( )_o$	corresponds to stagnation conditions
$( )_1$	conditions in front of normal shock
$( )_2$	conditions behind the normal shock
$(\dot{})$	rate of flow
$( )'$	perturbation quantity
$( )_\infty$	free-stream flow conditions
$( )_c$	corresponds to cavity conditions (See Figure 20)
$( )_D$	relates to diaphragm-reed system
$( )_E$	relates to conditions at the end of the tube
$( )_H$	relates to flow conditions across exit holes (Figure 20)
$( )_J$	corresponds to annular ram-air jet
$( )_s$	relates to static flow conditions at the generator exit holes
$( )_T$	relates to resonance tube conditions
$( )_w$	working equilibrium flow conditions

ABSTRACT

A combined experimental and analytical investigation was performed to understand the various fluid processes associated with the conversion of flow energy into electric power in a fluidic generator. Experiments were performed under flight-simulated laboratory conditions and results were compared with those obtained in the free-flight conditions. From these measurements, it was concluded that the mean mass flow critically controlled the output of the fluidic generator. Cross-correlation of the outputs of transducer data indicated the presence of a standing wave in the tube; therefore the mechanism of oscillation was an acoustic resonance tube phenomenon and did not represent the Helmholtz type of oscillation phenomenon.

On the basis of experimental results, a linearized model was constructed coupling the flow behavior of the jet, the jet-layer, the tube, the cavity, and the holes of the fluidic generator. The analytical results also showed that the mode of the fluidic power generator is an acoustical resonance phenomenon with the frequency of operation given by $f \simeq a/4L$, where f is the frequency of jet swallowing, a is the average speed of sound in the tube, and L is the length of the tube. Analytical results further indicated that oscillations in the fluidic generator are always damped and consequently there is a forcing of the system in operation.

I. INTRODUCTION

Periodic oscillations in jet flows impinging on solid surfaces have been observed over a range of flow conditions and geometrical variations (Reference 1). The oscillation phenomenon in such jet flows is very similar to that observed in axisymmetric cavity flows. Both experimental and analytical investigations of flows over cavities by V. Sarohia (References 2 to 6) have shown that the self-sustained oscillations are caused by the instability of the mean velocity profile and that they are amplified along the shear layer flow over the cavity. These previous investigations (Reference 5) further showed that the flow conditions downstream of the cavity influence the oscillation phenomenon as well as the shift of flow oscillations from one mode to another. The particular mode of the oscillation is determined by the phase of the propagating disturbance which attains the maximum value of the integrated amplification along the cavity shear layer.

Experiments performed on axisymmetric cavity flow oscillations showed the oscillation phenomenon depends on the external acoustic excitation (Reference 7). The jet edge-tone configuration in the fluidic electric power generator, as sketched in Figure 1, is similar to one in the axisymmetric cavity flow. However, the jet edge-tone oscillations will be modified by the resonance tube, reed-diaphragm system, and cavity surrounding the fluidic generator.

In flight, as indicated in Figure 1, air enters the fluidic power generator through the port located in the nose and leaves through the exhaust ports spaced uniformally around the circumferences of the ogive. During the passage of the air through the generator periodic air flow oscillations are produced by the jet interaction with the resonance tube. These flow oscillations are transmitted through a diaphragm and rod to reed that switches magnetic flux within the coil, thereby inducing a voltage at the coil terminals.

Little is known, however, about the manner in which the amplitude and the frequency of these flow oscillations influence the conversion of flow energy into electric power in the system shown in Figures 1 and 7. The understanding of various flow interactions that occur in the fluidic power generator is very essential to the efficiency of conversion of flow energy into electric power. The investigation reported here was designed to advance the understanding of these unanswered fundamental questions.

Laboratory measurements were made to relate to the free-flight performance of the fluidic generator. Based on the various underlying fluid processes associated with the production of oscillations in the generator, an analytic model which can predict the operation and the influence of configuration changes on generator performance was constructed. This model is the subject of the present report. The information obtained in this study has led to methods to improve the overall efficiency of the conversion of flow energy to electric power generation.

II. EXPERIMENTAL ARRANGEMENTS AND MEASUREMENTS

To enhance our understanding of the various flow processes responsible for the conversion of flow energy into electric power, two experimental setups were constructed. The bench test setup is shown in Figure 2. This facility could supply compressed air at various stagnation temperatures up to 700°F. The air was heated by passing it through an electric heater with a temperature control Variac as shown in Figure 2. This controlled-temperature air was accelerated through a convergent nozzle which was flushed with the inlet of the fluidic power generator. The total temperature and pressure in the settling chamber, along with static pressure at the inlet were measured and utilized to compute the rate of mean mass flow entering the fluidic generator.

The fluidic generator output, as indicated in Figure 3, was monitored on the oscilloscope as well as on the rms meter. An environment chamber was also built to vary the ambient static pressure around the fluidic generator. The cavity pressure p_c and ambient pressure p_∞ were monitored. Figure 3 also indicates the various electric outputs of the fluidic generator, such as the regulator output, the generator output, and the frequency output, which were recorded throughout this investigation.

Since the bench test setup, as shown in Figure 2, did not simulate the air flow around the generator, experiments were performed by placing the generator in the free-jet experimental test setup shown in Figure 4. The total stagnation inlet pressure, cavity pressure p_c, and the pressure at the exit holes, along with the output of the fluidic generator were measured at various flight-simulated flow conditions.

To determine the mechanism of operation of the fluidic generator, three 1/8-in. fast-response pressure transducers with a rise time of 2μsec and

a frequency response from 2 to 40,000 Hz were employed. One transducer was located at the base and the second was located flushed with the mouth of the tube to measure time varying pressure in the tube. The outputs of these transducers were cross-correlated on an all-digital-correlator. The third transducer was utilized to measure the cavity pressure fluctuations. Figures 5 and 6 show the physical locations of these transducers in the fluidic generator.

To determine the dynamic response and the natural frequency of operation of the generator diaphragm-reed system, an accelerometer was mounted to the reed as shown in Figure 3. The output of this accelerometer was recorded on an rms meter and displayed on an oscilloscope.

III. EXPERIMENTAL RESULTS

3.1 Calculations of Laboratory Conditions to Simulate Free-Flight Conditions

Given the altitude Z, the static conditions in front of the fluidic generator (denoted by subscript 1 in Figure 7) can be calculated using the U.S. Standard Atmosphere (Reference 8). To simplify calculations we use the geopotential altitude H, which equates the work required to lift a unit mass (under varying gravitational field) to Z with the work required to lift the same unit mass to H through a region with uniform gravity $g_o = 9.80655\ m/s^2$.

Transformation:

$$\text{From } Z \to H \qquad H = \frac{r_o Z}{r_o + Z} \ ; \ r_o = 6{,}356{,}766 m$$

$$T_\infty = \begin{cases} 288.15 - 0.0065H & 0<H<11{,}000m \\ 216.65 & 11{,}000<H<20{,}000 \\ 216.65 + 0.001\ (H-20{,}000) & 20{,}000<H<30{,}000 \end{cases} \qquad (1)$$

$$p_\infty = \begin{cases} 101{,}325.0\ \left(\frac{288.15}{T_\infty}\right)^{-5.2559} & 0<H<11{,}000m \\ 22{,}632.1 \exp\left[-1.5772\ (H-11{,}000)10^{-4}\right] & 11{,}000m<H<20{,}000m \\ 5{,}473.1\ \left(\frac{216.65}{T_\infty}\right)^{34.163} & 20{,}000m<H<30{,}000m \end{cases} \qquad (2)$$

$$\rho_\infty = \frac{M_o}{R^*}\frac{p_\infty}{T_\infty} = 3.4837\ \frac{p_\infty}{T_\infty}$$

where M_o is the molecular weight and R* is the universal gas constant. In these formulas T_∞ is obtained in K, p_∞ in newton per m^2, and ρ_∞ in kg/m^3.

The sonic velocity at point (1) $a_\infty = \sqrt{\gamma R T_\infty}$, for air $\gamma = 1.4$, $\frac{R^*}{M_o} = 287.05$ joule/(kg K).

$$a_\infty = \sqrt{401.87\ T_\infty} = 20.046\sqrt{T_\infty},\ T_\infty \text{ in kelvins} \qquad (3)$$

$$M_1 = \frac{U}{a_0},\ U \text{ is the fluidic generator velocity in m/s.}$$

Moving across the shock to point (2)

$$\frac{p_2}{p_1} = \frac{2\gamma M_1^2 - (\gamma-1)}{\gamma+1} = \frac{7M_1^2 - 1}{6}$$

$$\frac{p_{o2}}{p_1} = \left(\frac{(\gamma+1)M_1^2}{2}\right)^{\gamma/\gamma-1}\left(\frac{\gamma+1}{2\gamma M_1^2-(\gamma-1)}\right)^{\frac{1}{\gamma-1}} = \left(\frac{6M_1^2}{5}\right)^{\frac{7}{2}}\left(\frac{6}{7M_1^2-1}\right)^{\frac{5}{2}}$$

$$M_2^2 = \frac{(\gamma-1)M_1^2 + 2}{2\gamma M_1^2 - (\gamma-1)} = \frac{M_1^2 + 5}{7M_1^2 - 1} \qquad (4)$$

$$\frac{T_2}{T_1} = \frac{[2\gamma M_1^2 - (\gamma-1)][(\gamma-1)M_1^2 + 2]}{(\gamma+1)^2 M_1^2} = \frac{(7M_1^2-1)(M_1^2+5)}{36M_1^2}$$

The important variable is the driving pressure Δp, which is the difference of the stagnation pressure p_{o2} at the front of the fluidic generator minus the cavity pressure around the resonator ($\Delta p = p_{o2} - p_c$). To transform free flight to the bench test, it was assumed that $\Delta p = p_{o2} - p_c = p_3 - p_\infty$ (see Figure 3). Because of difficulties in estimating p_c in free flight, a similar idea was tried by equating $(p_o - p_s)$ or $p_{o2} - p_s = p_3 - p_\infty$ (see Figures 3 and 7).

Therefore, by knowing the altitude Z, and the fluidic generator velocity U, $M_1 = U/a_\infty(Z)$ at that altitude can be calculated from relations (1) to (3) above. Using shock relation (4), the stagnation pressure in front of the generator p_{o2} and therefore the laboratory conditions needed to simulate the flight can be computed. A computer program was developed, which is attached in Appendix A along with some sample calculations.

3.2 Comparison of Bench Results With Free-Jet Results

To determine the influence of flight flow around the fluidic generator, bench test results (Figure 2) were compared with those obtained in the free-jet facility (Figure 4). The driving pressure ($p_o - p_\infty$) was kept constant. The pressure p_3 in Figure 3 is assumed equal to the stagnation pressure p_o in front of the generator in the free-jet facility shown in Figure 2. Typical results of such a comparison are shown in Figure 8. As is evident in these results, for a given differential pressure $p_o - p_\infty$, the bench test output was always greater than that obtained by the free-jet test results. It should be noted that for this comparison the same generator was utilized. A comparison with two other generators was also made, and similar results were obtained. These results indicated that the fluidic generator output did not depend upon the differential pressure $p_o - p_\infty$.

Upon careful analysis of other experimental data, i.e., cavity pressure p_c as a function of the driving pressure $p_o - p_\infty$, it was observed that for a given $(p_o - p_\infty)$, the cavity pressure p_c was always high in the free-jet case as compared with the bench tests. These results are shown in Figure 9. Therefore, in Figure 10, the fluidic generator output was plotted as a function of $(p_o - p_c)$ and the agreement between free-jet and bench test results was excellent.

From this study, it is therefore concluded that the most important parameter that controls the fluidic generator output is not $p_o - p_\infty$ but rather $p_o - p_c$, the differential pressure between the total stagnation pressure in front of the generator and the cavity pressure.

3.3 Comparison of Laboratory Results With Flight Data

Apart from getting the physical insight needed to model the fluid electric power generator from the above experiments, an attempt was made to correlate the laboratory tests with those obtained from flight data. The flight data was provided to JPL by Harry Diamond Laboratories. From the knowledge of the flight velocity and altitude, the laboratory flow conditions were calculated as discussed above in Section 3.1 and Appendix A.

The results of such a comparison are shown in Figure 11. Since p_c was not available in the flight data, the static pressure behind the oblique shock was equated to p_c. As is evident from Figure 11, the comparison with the bench test results is very poor. The discrepancy in such a comparison may have been caused by the assumption that cavity pressure p_c in flight is equal to p_∞ around the generator close to the holes. Flight measurements of p_c are needed to enhance our understanding to better correlate the flight data with laboratory test results. Furthermore, it should be noted that the absolute pressures in the bench facility and in flight are not identical.

3.4 Mass Flow Measurements

To better understand the performance of the operation of the fluidic generator, detailed measurements of the mass flow through the fluidic generator were determined as a function of various operating pressures. The influence of the exit hole area on generator performance was also determined.

The calculations utilized to determine the mass flow rate through the fluidic device are shown in Appendix B. Figure 12 indicates the mass flow rate normalized with cavity pressure and plotted as a function of pressure ratio p_s/p_c where p_s is the static pressure at the holes, which under conditions of no external flow is the same as atmospheric pressure p_∞. Tables 1 - 4 give the measured data along with the calculated mass flow rate and computed nozzle flow coefficients. The mass flow rate, and consequently, generator output drop for a given pressure ratio p_s/p_c when the holes are closed partially. However, if the mass flow rate is normalized with stagnation pressure p_o, then the results shown in Figure 12 collapse into a single curve as shown in Figure 13. Results of Figures 12 and 13 clearly indicate the importance of the cavity pressure p_c in controlling the mass flow rate through the generator. Any changes in the geometry of the holes will influence p_c which in turn modifies the mass flow rate and the output of the fluidic generator.

To determine the influence of the ambient pressure $p_s = p_\infty$ in the bench test on mass flow rate through the generator, the environment chamber shown in Figure 3 was employed. Figure 14 shows the typical results of such an investigation. For all the exit holes opened, the mass flow rate $\dot{m}$ was independent of the ambient pressure for a given stagnation pressure p_o and p_c. These results strongly suggest that the mass flow rate under subsonic flow conditions through the generator critically depends upon the differential

pressure ($p_o - p_c$).

The influence of the Reynolds number calculated on the nozzle velocity coefficient is shown in Figure 15. These results showed that the changes in the exit hole area did not significantly modify the ram-jet flow responsible for generating pressure fluctuations in the table. Tables 1 - 4 give the output of the nozzle velocity coefficient for various operating conditions.

3.5 Mechanism of Fluidic Generator Operation

To correctly model the operation of the fluidic generator, important information was needed to determine the mechanism responsible for pressure fluctuations in the tube. As shown in Figures 5 and 6, the pressure transducer output was cross-correlated to determine any standing waves in the tube.

The instant pressure transducer output at the mouth and base of the resonance tube of the fluidic generator is shown in Figure 16. To mount the transducer at the base, the diaphragm was replaced by a solid plate. Figure 16 also shows the auto and cross-correlations of these microphone signals. As is evident, the peak of the cross-correlation signal was delayed by 1/4 the time period of the pressure fluctuation frequency in the tube. This frequency is the fundamental tube resonance frequency given by $f=a/4L$, where L is the length of the tube. From these measurements, it is concluded that the pressure fluctuations, and consequently the oscillations of the diaphragm-reed system of the fluidic generator, result from an acoustic resonance phenomenon in the tube. These measurements did not support the Helmholtz type of oscillation phenomenon in the generator as has been commonly assumed in the past.

The influence of mass flow rate on the output of the pressure

oscillations at the base of the resonance tube (so called since the frequency of pressure oscillations is at the fundamental resonance tube frequency) was studied. Results in Figure 17 indicated a linear relationship between the mass flow rate and the rms pressure fluctuations at the base of the cavity. This linear relationship suggests that the annular ram-air jet is periodically swallowed by the tube at the frequency of resonance tube oscillation. This phenomenon, discussed in detail in Reference 9, is called the regurgitant mode of resonance tube operation. Furthermore, since mass flow rate is proportional to $(p_o - p_c)$ as discussed in Section 3.4, the magnitude of the pressure fluctuations at the base of the resonance tube is directly related to this differential pressure.

3.6 Accelerometer Output

Other experimental information needed to properly model the fluidic generator required us to determine the transient response of the fluidic diaphragm-reed subsystem of the fluidic generator. The accelerometer output was compared with the generator output at different pressures, as shown in Figure 18. Both outputs were at the resonance tube frequency. The transient response of the diaphragm-reed system is shown in Figure 19. The present measurements show the natural frequency of oscillation of the diaphragm-reed subsystem to be about 1412 Hz. The information shown in Figures 18 and 19 was utilized in an analytical model employed to compute the performance of this fluidic generator.

IV. ANALYTICAL RESULTS

4.1 Governing Equations of Fluidic Generator Operation

Since the operation of the fluidic generator performance critically depends upon the mass flow rate through the system, the governing equations which couple the annular ram-air jet, ring-tone jet-layer, cavity and resonance tube have been written in terms of nomenclature and Figure 20. The governing equations can be written as

$$I_J \frac{d\dot{m}_J'}{dt} + \left(\frac{dp_c}{d\dot{m}_J}\right)_w \dot{m}_J' = - p_c' \qquad \text{Annular Jet}$$

$$I_T \frac{d\dot{m}_T'}{dt} + B_T \dot{m}_T' = p_T' - p_c' \qquad \text{Jet Layer}$$

$$\frac{a M}{A_T} \dot{m}_T' = - p_T' \qquad \text{Resonance Tube}$$

$$\frac{dp_c'}{dt} = \frac{a^2}{V_c} \dot{m}_c' = \frac{a^2}{V_c} (\dot{m}_J' - \dot{m}_H' + \dot{m}_T') \qquad \text{Cavity}$$

$$I_H \frac{d\dot{m}_H}{dt} + \left(\frac{dp_c}{d\dot{m}_H}\right)_w \dot{m}_H' = p_c' \qquad \text{Holes}$$

where $(\,)'$ denotes acoustical oscillations and $\left(\frac{dp_c}{dm_j}\right)_w$ denotes the variation of the cavity pressure with the jet mass flow at the working (w) point of the fluidic generator. For detailed derivation of the equations, see Appendix C.

For solutions of the form e^{zt}, $z = \sigma + i\omega$, in vector notation we write

$$\begin{pmatrix} p'_T \\ p'_c \\ \dot{m}'_J \\ \dot{m}'_H \\ \dot{m}'_T \end{pmatrix} = \begin{pmatrix} \hat{p}_T \\ \hat{p}_c \\ \hat{\dot{m}}_J \\ \hat{\dot{m}}_H \\ \hat{\dot{m}}_T \end{pmatrix} \exp(zt)$$

where

$$z = \sigma + i\omega, \quad M = \frac{1 + R \exp\left[-\frac{2zL}{a}\right]}{1 - R \exp\left[-\frac{2zL}{a}\right]}$$

One finds in matrix notation

$$\begin{pmatrix} 0 & \frac{V_c}{a^2} z & -1 & 1 & -1 \\ 0 & 1 & I_J z + \left(\frac{dp_c}{d\dot{m}_J}\right)_w & 0 & 0 \\ 0 & -1 & 0 & I_H z + \left(\frac{dp_c}{d\dot{m}_H}\right)_w & 0 \\ -1 & 1 & 0 & 0 & I_T z + B_T \\ 1 & 0 & 0 & 0 & \frac{a M}{A_T} \end{pmatrix} \begin{pmatrix} \hat{p}_T \\ \hat{p}_c \\ \hat{\dot{m}}_J \\ \hat{\dot{m}}_H \\ \hat{\dot{m}}_T \end{pmatrix} = 0$$

Introducing nondimensional variables,

$$\alpha_J = I_J \frac{A_T}{L} \;,\; \beta_J = \frac{A_T}{a}\left(\frac{dp_c}{d\dot{m}_J}\right)_w$$

$$\alpha_H = I_H \frac{A_T}{L} \;,\; \beta_H = \frac{A_T}{a}\left(\frac{dp_c}{d\dot{m}_H}\right)_w$$

$$\alpha_T = I_T \frac{A_T}{L} \;,\; \beta_T = \beta_T \frac{A_T}{a}$$

$$\zeta = \frac{z\,L}{a} \;,\; K = \frac{V_c}{A_T L} \;,\; \mu_J = \frac{\hat{\dot{m}}_J}{\hat{\dot{m}}_T} \;;\; \mu_H = \frac{\hat{\dot{m}}_H}{\hat{\dot{m}}_T}$$

where

L = Length of the resonance tube

A_T = Area of the resonance tube

a = Speed of sound = <u>average</u>

The governing equation can be written

$$\begin{pmatrix} 0 & K\zeta & -1 & 1 & -1 \\ 0 & 1 & \alpha_J\zeta+\beta_J & 0 & 0 \\ 0 & -1 & 0 & \alpha_H\zeta+\beta_H & 0 \\ -1 & 1 & 0 & 0 & \alpha_T\zeta+\beta_T \\ 1 & 0 & 0 & 0 & M \end{pmatrix} \begin{pmatrix} \sigma_T \\ \sigma_c \\ \mu_J \\ \mu_H \\ 1 \end{pmatrix} = 0$$

For solution, the determinant should be zero

$$\begin{vmatrix} 0 & K\zeta & -1 & 1 & -1 \\ 0 & 1 & \alpha_T\zeta+\beta_j & 0 & 0 \\ 0 & -1 & 0 & \alpha_H\zeta+\beta_H & 0 \\ -1 & 1 & 1 & 1 & \alpha_T\zeta+\beta_T \\ 1 & 0 & 0 & 0 & M \end{vmatrix} = 0$$

which results in the equation

$$F(\zeta) \equiv M + \alpha_T\zeta+\beta_T\,[K\zeta(\alpha_j\zeta+\beta_j)(\alpha_H\zeta+\beta_H)+(\alpha_j\zeta+\beta_j)+(\alpha_H\zeta+\beta_H)]$$
$$+ (\alpha_j\zeta+\beta_j)(\alpha_H\zeta+\beta_H) = 0 \qquad (5)$$

$$\text{with } M = \frac{e^{\zeta}+Re^{-\zeta}}{e^{\zeta}-Re^{-\zeta}}\,, \quad R = \frac{1-\phi+\eta\zeta\left(1+\dfrac{\Omega^2}{\zeta^2}\right)}{1+\phi+\eta\zeta\left(1+\dfrac{\Omega^2}{\zeta^2}\right)}$$

$$\phi = \frac{\rho a A_D^2}{A_T f_D}\,, \quad \eta = \frac{m_D\, a}{f_D\, L}, \quad \Omega = \frac{L}{a}\sqrt{\frac{k_D}{m_D}}$$

where D denotes the diaphragm-reed conditions.

For the solution of the above equation, we need to calculate the constants first.

4.2 Calculations of Constants

For these calculations, the dimensions of the fluidic generator have been used as follows:

Diaphragm-Reed

For these calculations, data in Figure 19 has been utilized.

$$\eta = \frac{m_D\, a}{f_D\, L} = 22.5$$

$$\zeta = 0.946$$

ϕ is unknown

Jet

$$\alpha_J = \frac{h\, A_T}{A_J\, L} = .5243$$

$$\beta_J = .006\, \frac{pc}{\dot{m}}\, \frac{7\left[1-\left(\frac{p_c}{p_o}\right)^{2/7}\right]}{5-6\left(\frac{pc}{p_o}\right)^{2/7}} \quad \text{for } p_c/p_o > 0.528$$

$$= \infty \text{ for } p_c/p_o < 0.528$$

Holes

$$\alpha_H = \frac{d_H\, A_T}{A_H L} = .0936$$

$$\beta_H = .006\, \frac{pc}{\dot{m}}\, \frac{7\left[1-(p_s/p_c)^{2/7}\right]}{2-(p_s/p_c)^{2/7}} \quad \text{for } \frac{p_c}{p_o} > 0.528$$

or

$$\beta_H = 0.0006\, \frac{p_c}{\dot{m}} \text{ for } \frac{p_s}{p_c} < 0.528$$

Jet Layer

$$\alpha_T = \frac{hA_T}{\ell\, W\, L} = 0.0132$$

$$\beta_T = \frac{A_T\, \dot{m}}{\rho\, a\, \ell^2\, W^2} = 349\, \dot{m}$$

Cavity

$$K = \frac{V_c}{A_T L} = 14.5831$$

Independent Variables

$$\zeta = (\sigma+i\omega)\, \frac{L}{a} = 1.095 \times 10^{-4}\ (\sigma+i\omega)$$

4.3 Numerical Results

A computer program was developed to solve the equation (5) as developed in 3.1 above with the above physical constant. The computer program is listed in Appendix D. The input variables were the working conditions as follows:

p_o stagnation pressure in front of the oscillations

p_c cavity pressure

p_s static pressure close to the exit holes

$\dot{m}$ mass flow rate

The solution of equation (5), $F(\zeta) = 0$ was found for the following cases:

(a) Fixed resonant frequency of the diaphragm (Ω) for various ϕ at the operating conditions of the fluidic generator.

(b) Fixed ϕ and varied r for these three operating conditions.

The output of these results are shown in the following table.

p_o	p_c	p_s	$\dot{m}$	η	Ω	$\frac{\omega L}{a}$ ϕ=0	$\frac{\omega L}{a}$ ϕ=1	$\frac{\sigma L}{a}$ β=0	$\frac{\sigma L}{a}$ β=1
20.38	15.147	14.32	.0270	22.527	0.946	1.60	1.63	-.095	-.092
						4.67	4.68	-.093	-.093
26.559	16.093	14.32	.0397	22.527	1.5	1.59	1.70	-.137	-.101
						4.61	4.68	-.138	-.137
				22.527	.946	1.59	1.63	-.131	-.133
						4.67	4.68	-.138	-.137
				22.527	.5	1.59	1.62	-.137	-.135
						4.61	4.67	-.138	-.137
				10	.946	1.60	1.68	-.137	-.137
				1	.946	1.60	2.07	-.137	-2.94
						4.61	4.87	-.130	-.172
32.781	17.082	14.32	.0505	22.527	.946	1.60	1.63	-.175	-.169
						4.66	4.67	-.175	-.175

It is evident from the numerical results that

(a) The natural frequency of the system is controlled by resonance conditions of the tube i.e., $\omega L/a = \pi/2, 3\pi/2$

(b) Oscillations are always damped

(c) To keep the system in operation, forcing of the system is needed.

V. DISCUSSION AND CONCLUSIONS

The experimental work performed to develop the mathematical model to predict generator performance has shown that the mode of cavity operation is governed by the standing acoustic resonance phenomenon in the tube. In this mode of operation, the annular jet is periodically swallowed and subsequently discharged by the resonance tube at the fundamental tube resonance frequency (Reference 9). The basic mechanism of conversion of flow energy to acoustic power (and subsequently to mechanical motion) by the fluidic generator is critically dependent on the jet mass flow and the geometry of the gap between the nozzle exit and the resonating cavity. The basic understanding of the physical processes in this region under a simulated high altitude flow configuration is essential for designing the fluidic generator with optimum performance. More work is needed in this area to improve the efficiency of the conversion of fluid energy to electric power under high-altitude flight conditions.

The comparison of laboratory test results with the flight test data (Figure 11) shows that the existing laboratory tests do not correctly simulate the performance of the fluidic generator at altitude. A close look at the flow field in the annular jet showed that the flow becomes supersonic inside the generator in flight, as compared with subsonic flow in the existing laboratory simulation facilities. To correctly simulate flight, a vacuum facility is needed to simulate both the high-altitude mass flow through the fluidic electric generator and the static flow pressures in and around the fluidic generator.

ACKNOWLEDGEMENTS

This work was performed for the Harry Diamond Laboratories under Task Order RD-182, Amendment No. 83, MIPR No. R-80-070 dated July 9, 1980. The authors extend their gratitude to Mr. Richard Deadwyler of Harry Diamond Laboratories for many valuable technical suggestions throughout the program. The authors are grateful to Paul F. Massier for his guidance and support in this research and to Wayne Bixler, Stanley Kikkert, and Joseph Godley for technical assistance in conducting the experiments.

REFERENCES

1. K. Karamechti et al., NASA Headquarters Conference on Basic Aeronautics Noise Research, NASA Special Publication 207, pp. 275-304, 1969.

2. V. Sarohia, "Experimental Investigation of Oscillations in Flows Over Shallow Cavities," AIAA Journal, Vol. 15, No. 7, pp. 984-991, July 1977.

3. V. Sarohia and P. F. Massier, "Investigation of Pressure Oscillations in Axisymmetric Cavity Flows," Harry Diamond Laboratories Report No. HDL-CR-77-025-1, September 1977.

4. V. Sarohia and P. F. Massier, "Effect of Angle of Attack on Cavity Flow Oscillations," Harry Diamond Laboratories Report No. HDL-CR-78-025-1, October 1978.

5. V. Sarohia, "On Prediction of Oscillations Over Shallow Cavities" (in preparation).

6. V. Sarohia, "Spanwise Structures of Axisymmetric Cavity Shear Flows," presented at 31st meeting of the American Physical Society, November 1978.

7. V. Sarohia, "Experimental and Analytical Investigation of Oscillations in Flows and Cavities," Ph.D. Thesis, California Institute of Technology, Pasadena, California, March 1975.

8. U. S. Standard Atmosphere, National Oceanic and Atmospheric Administration, Washington, D. C., October 1976.

9. V. Sarohia and L. H. Back, "Experimental Investigation of Flow and Heating in a Resonance Tube," Journal of Fluid Mechanics 94, Part 4, 649-672.

APPENDIX A

CALCULATIONS OF LABORATORY CONDITIONS TO SIMULATE FLIGHT CONDITIONS

ORIGINAL PAGE IS
OF POOR QUALITY

```
FORTRAN IV-PLUS V02-51          12:24:12     15-OCT-79          PAGE 1
ATM1.FTN        /TR:BLOCKS/WR

      C  THIS PROGRAM DETERMINES CONDITIONS AT THE END OF THE
      C  FLUIDIC GEN. GIVEN THE VELOCITY AND ALTITUDE OF THE MISSILE,
      C  FROM THESE CONDITIONS AT THE END OF THE FLUIDIC GEN.
      C  THE CONDITIONS UPSTREAM IN THE AIR STRAIGHTENING SECTION ARE DETERMINED
      C  PS    = STATIC SURFACE PRESSURE OF OGIVE AT PT. 2.
      C  P     = PRESSURE (N/M**2) AT DIFFERENT POINTS.
      C  PO    = STAGNATION PRESSURE (N/M**2) AT DIFFERENT POINTS.
      C  T     = TEMPERATURE (KELVIN) AT DIFFERENT POINTS.
      C  TO    = TOTAL TEMPERATURE (KELVIN) AT DIFFERENT POINTS.
      C  M     = MACH NO. AT DIFFERENT POINTS.
      C  PSI   = P IN (PSI)
      C  TR    = T IN (R)
      C  PT. 1 = CONDITIONS UPSTREAM OF BOW SHOCK WAVE.
      C      2 = CONDITIONS DOWNSTREAM OF BOW SHOCK (ACTUAL FLIGHT COND.)
      C           JUST UPSTREAM OF FLUIDIC GEN.
      C  PT. 3 = CONDITIONS JUST UPSTREAM OF FLUIDIC GEN. IN LAB.
      C           APPARATUS.
      C  PT. 4 = CONDITIONS IN THE AIR STRAIGHTENING SECTION OF LAB.
      C           APPARATUS.
0001           DIMENSION HEAD(2)
0002           DOUBLE PRECISION P(4),T(4),PSI(4),TR(4),PO(4),TO(4),
     1     CP(2),CV(2),M(4),K,A3,A4,RHO(4),PS,X
0003           DATA A3/1.266769/,A4/182.41469/
0004           DATA HEAD/4HAIR ,4HHEL./,CP/3.5,2.5/,CV/2.5,1.5/
0005           DATA XSAVE/1.0E+20/,PCONV/1.45038E-04/
0006           TYPE *,'INPUT VELOCIYT(M/S),ALTITUDE(M)'
0007           ACCEPT *,V,Z
0008           CALL ATM76(Z,T(1),P(1),RHO(1))
0009           A = 20.046803 * SQRT(T(1))
0010           M(1) = V / A
0011           PO(1) = P(1) * (1. + .2*M(1)*M(1))**3.5
0012           TO(1) = T(1) * (1. + .2*M(1)*M(1))
      C
      C  CALC. MACH NO. OF MISSILE.
      C
0013           A = 20.046803 * SQRT(T(1))
0014           V = M(1) * A
0015           IF (M(1).GT.1.)GO TO 5
      C
      C  SUBSONIC FLIGHT
      C
0016           T(2) = T(1)
0017           P(2) = P(1)
0018           M(2) = M(1)
0019           PO(2) = PO(1)
0020           TO(2) = TO(1)
0021           PS = P(2) + .23 * (PO(2) - P(2))
0022           GO TO 6
0023     5     CONTINUE
      C
      C  CALC. OF CONDITIONS AT FLUIDIC GEN. FROM ATMOSPHERIC CONDITIONS
      C  AND VELOCITY OF MISSILE,SAME PROBLEM AS CALC. DOWNSTREAM CONDITIONS
      C  OF A NORMAL SHOCK WAVE FROM UPSTREAM CONDITIONS.
      C
0024           X = M(1) * M(1)
0025           P(2) = P(1) * (7.*X - 1.) / 6.
```

```
0026            PO(2) = P(1) * (1.2*X)**3.5 * (P(1)/P(2))**2.5
0027            M(2) = SQRT((X+5.) / (7.*X-1.))
0028            T(2) = T(1) * (7.*X-1.) * (X+5.) / (36.*X)
0029            TO(2) = T(2) * (1. + .2*M(2)*M(2))
        C
        C  CALC OF CONDITIONS JUST UPSTREAM OF FLUIDIC GEN. FOR
        C  THE LAB APPARATUS FROM THE ACTUAL UPSTREAM CONDITIONS
        C  REQUIRED CONSTRAINTS ARE:DRIVING PRESSURE OF THE GEN.
        C  MUST BE THE SAME.
        C                              :THE STAGNATION TEMP. OF THE ATMOSPHERE
        C  JUST BEFORE THE FLUIDIC GEN. (PT. 2) MUST EQUAL THE STAGNATION
        C  TEMP. AT PT. 3.
        C
0030    6       DO 40 L=1,2
0031            K = CP(L) / CV(L)
0032            P(3) = 101325.0
0033            PO(3) = PO(2) + P(3) - PS
0034            M(3) = SQRT( 2./(K - 1.) * ((PO(3)/P(3))**((K - 1.)/K) - 1.) )
0035            STORE = .5*(K - 1.)*M(3)*M(3)
0036            TO(3) = TO(2)
0037            T(3) = TO(3) / (1. + STORE)
0038            EXPON = .5 * (K + 1.) / (K - 1.)
0039            CRIT = A4/(A3*M(3)) * (1. + STORE)/(.5*(K+1.))**EXPON
0040            X = (1. / (.5*(K+1.)))**EXPON
0041            M(4) = X / CRIT
0042            PO(4) = PO(3)
0043            TO(4) = TO(3)
0044            P(4) = PO(4) / (1. + .5*(K-1.)*M(4)*M(4))**(K/(K-1))
0045            T(4) = TO(4) / (1. + .5*(K-1.)*M(4)*M(4))
        C
        C  PRINT OUT RESULTS.
        C
0046            TYPE 100,HEAD(L),V,Z
0047    100     FORMAT(/,1X,'GAS IN LAB APPARATUS: ',A4/2X,'VELOCITY = ',F8.2,
              1 ' (M/S)'/2X,'ALTITUDE = ',F9.2,' (M)',//
              2 31X,'STAG.                STAG.',/
              3 1X,'PT.  TEMP.(K)  P (N/M**2)   TEMP.(R)  TEMP.(R)   P (PSI)',
              4 '   P (PSI)     MACH NO.')
0048            DO 30 I=1,4
0049            TR(I)  = 1.8 * T(I)
0050            PSI(I) = PCONV * P(I)
0051            TRO = 1.8 * TO(I)
0052            PSIO = PCONV * PO(I)
0053    30      WRITE(6,110)I,T(I),P(I),TRO,TR(I),PSIO,PSI(I),M(I)
0054    110     FORMAT(1X,I2,2X,F8.2,F13.2,2F10.2,2F11.5,F12.6)
0055            X = (PO(2) - PS) * PCONV
0056            WRITE(6,120)X
0057    120     FORMAT(2X,'DRIVING PRESS. (P(4)-P(ATM.)) = ',F7.3)
0058    40      CONTINUE
0059           STOP
0060           END
```

```
FORTRAN IV-PLUS V02-51          12:28:52     15-OCT-79          PAGE 4
ATM1.FTN        /TR:BLOCKS/WR

0001            SUBROUTINE ATM76(Z,T,P,RHO)
      C
      C  SUBROUTINE ATM76 GENERATES THE ATMOSPHERIC CONDITIONS
      C  T,P,RHO GIVEN THE ALTITUDE ACCORDING TO THE U.S. STANDARD
      C  ATMOSPHERE,1976.
      C
0002             DOUBLE PRECISION T,P,RHO,MWT,G,R,R0,Z,H
0003            DATA R0/6356766./,MWT/28.9655/,G/9.80655/,R/8314.32/
0004            H = R0 * Z / (R0 + Z)
0005            IF (H.LE.11000.)GO TO 10
0006            IF (H.LE.20000.)GO TO 20
0007            IF (H.LE.32000.)GO TO 30
0008            TYPE *,'ALTITUDE IS TOO HIGH'
0009            RETURN
0010    10      T = 288.15 - .0065 * H
0011            P = 101325.0 * (288.15 / T)**((-1.)*G*MWT/(R*.0065))
0012            GO TO 40
0013    20      T = 216.65
0014            P = 22632.4 * EXP((-1.)*G*MWT*(H-11000.)/(R*216.65))
0015            GO TO 40
0016    30      T = 216.65 + .001 * (H - 20000.)
0017            P = 5475.05 * (216.65 / T)**(G*MWT/R)
0018    40      RHO = MWT*P / (R*T)
0019            RETURN
0020            END
```

```
FORTRAN IV-PLUS V02-51          12:28:52     15-OCT-79          PAGE 5
ATM1.FTN        /TR:BLOCKS/WR

PROGRAM SECTIONS

NUMBER    NAME        SIZE                    ATTRIBUTES

  1       $CODE1   000474    158              RW,I,CON,LCL
  2       $PDATA   000136     47              RW,D,CON,LCL
  4       $VARS    000050     20              RW,D,CON,LCL

ENTRY POINTS

 NAME    TYPE  ADDRESS     NAME    TYPE  ADDRESS     NAME    TYPE  ADDRESS     NAME

 ATM76         1-000000

VARIABLES

 NAME    TYPE  ADDRESS     NAME    TYPE  ADDRESS     NAME    TYPE  ADDRESS     NAME

 G       R*8   4-000010    H       R*8   4-000040    MWT     R*8   4-000000    P
 RHO     R*8   F-000010*   R0      R*8   4-000030    T       R*8   F-000004*   Z
```

```
 RUN ATM1
 INPUT VELOCIYT(M/S),ALTITUDE(M)
199.,4209.

GAS IN LAB APPARATUS: AIR
 VELOCITY =    199.00 (M/S)
 ALTITUDE =    4209.00 (M)

                                STAG.                    STAG.
PT.   TEMP.(K)   P (N/M**2)    TEMP.(R)   TEMP.(R)    P (PSI)     P (PSI)      MACH NO.
 1     260.81      60000.78     504.93     469.46    11.22968     8.70239     0.614676
 2     260.81      60000.78     504.93     469.46    11.22968     8.70239     0.614676
 3     270.73     101325.00     504.93     487.31    16.64199    14.69597     0.425257
 4     280.52     114741.60     504.93     504.93    16.64199    16.64189     0.002850
 DRIVING PRESS. (P(4)-P(ATM.)) =    1.946

GAS IN LAB APPARATUS: HEL.
 VELOCITY =    199.00 (M/S)
 ALTITUDE =    4209.00 (M)

                                STAG.                    STAG.
PT.   TEMP.(K)   P (N/M**2)    TEMP.(R)   TEMP.(R)    P (PSI)     P (PSI)      MACH NO.
 1     260.81      60000.78     504.93     469.46    11.22968     8.70239     0.614676
 2     260.81      60000.78     504.93     469.46    11.22968     8.70239     0.614676
 3     266.91     101325.00     504.93     480.43    16.64199    14.69597     0.391152
 4     280.52     114741.62     504.93     504.93    16.64199    16.64189     0.002585
 DRIVING PRESS. (P(4)-P(ATM.)) =    1.946
TTO  --  STOP

>RUN ATM1


 INPUT VELOCIYT(M/S),ALTITUDE(M)
176.9,4150.5

GAS IN LAB APPARATUS: AIR
 VELOCITY =    176.90 (M/S)
 ALTITUDE =    4150.50 (M)

                                STAG.                    STAG.
PT.   TEMP.(K)   P (N/M**2)    TEMP.(R)   TEMP.(R)    P (PSI)     P (PSI)      MACH NO.
 1     261.19      60461.39     498.17     470.14    10.73977     8.76920     0.546016
 2     261.19      60461.39     498.17     470.14    10.73977     8.76920     0.546016
 3     269.10     101325.00     498.17     484.38    16.21331    14.69597     0.377305
 4     276.76     111786.15     498.17     498.17    16.21331    16.21324     0.002548
 DRIVING PRESS. (P(4)-P(ATM.)) =    1.517

GAS IN LAB APPARATUS: HEL.
 VELOCITY =    176.90 (M/S)
 ALTITUDE =    4150.50 (M)

                                STAG.                    STAG.
PT.   TEMP.(K)   P (N/M**2)    TEMP.(R)   TEMP.(R)    P (PSI)     P (PSI)      MACH NO.
 1     261.19      60461.39     498.17     470.14    10.73977     8.76920     0.546016
 2     261.19      60461.39     498.17     470.14    10.73977     8.76920     0.546016
 3     266.10     101325.00     498.17     478.97    16.21331    14.69597     0.346783
 4     276.76     111786.16     498.17     498.17    16.21331    16.21324     0.002315
 DRIVING PRESS. (P(4)-P(ATM.)) =    1.517
TTO  --  STOP
```

```
 RUN ATM1
 INPUT VELOCIYT(M/S),ALTITUDE(M)
185.7,3195.4

GAS IN LAB APPARATUS: AIR
 VELOCITY =   185.70 (M/S)
 ALTITUDE =   3195.40 (M)

                              STAG.                    STAG.
PT.  TEMP.(K)  P (N/M**2)    TEMP.(R)  TEMP.(R)  P (PSI)     P (PSI)     MACH NO.
 1    267.39     68397.19     512.19    481.30  12.33323     9.92019    0.566492
 2    267.39     68397.19     512.19    481.30  12.33323     9.92019    0.566492
 3    275.04    101325.00     512.19    495.06  16.55401    14.69597    0.415938
 4    284.55    114135.07     512.19    512.19  16.55401    16.55392    0.002792
 DRIVING PRESS. (P(4)-P(ATM.)) =   1.858

GAS IN LAB APPARATUS: HEL.
 VELOCITY =   185.70 (M/S)
 ALTITUDE =   3195.40 (M)

                              STAG.                    STAG.
PT.  TEMP.(K)  P (N/M**2)    TEMP.(R)  TEMP.(R)  P (PSI)     P (PSI)     MACH NO.
 1    267.39     68397.19     512.19    481.30  12.33323     9.92019    0.566492
 2    267.39     68397.19     512.19    481.30  12.33323     9.92019    0.566492
 3    271.32    101325.00     512.19    488.37  16.55401    14.69597    0.382521
 4    284.55    114135.08     512.19    512.19  16.55401    16.55392    0.002533
 DRIVING PRESS. (P(4)-P(ATM.)) =   1.858
TTO  --  STOP

>RUN ATM1
 INPUT VELOCIYT(M/S),ALTITUDE(M)
203.4,1615.4

GAS IN LAB APPARATUS: AIR
 VELOCITY =   203.40 (M/S)
 ALTITUDE =   1615.40 (M)

                              STAG.                    STAG.
PT.  TEMP.(K)  P (N/M**2)    TEMP.(R)  TEMP.(R)  P (PSI)     P (PSI)     MACH NO.
 1    277.65     83369.21     536.84    499.77  15.53180    12.09170    0.608913
 2    277.65     83369.21     536.84    499.77  15.53180    12.09170    0.608913
 3    284.45    101325.00     536.84    512.01  17.34485    14.69597    0.492382
 4    298.24    119587.41     536.84    536.83  17.34485    17.34472    0.003261
 DRIVING PRESS. (P(4)-P(ATM.)) =   2.649

GAS IN LAB APPARATUS: HEL.
 VELOCITY =   203.40 (M/S)
 ALTITUDE =   1615.40 (M)

                              STAG.                    STAG.
PT.  TEMP.(K)  P (N/M**2)    TEMP.(R)  TEMP.(R)  P (PSI)     P (PSI)     MACH NO.
 1    277.65     83369.21     536.84    499.77  15.53180    12.09170    0.608913
 2    277.65     83369.21     536.84    499.77  15.53180    12.09170    0.608913
 3    279.11    101325.00     536.84    502.40  17.34485    14.69597    0.453438
 4    298.24    119587.43     536.84    536.83  17.34485    17.34472    0.002947
 DRIVING PRESS. (P(4)-P(ATM.)) =   2.649
TTO  --  STOP
```

APPENDIX B

CALCULATIONS OF MASS FLOW THROUGH THE FLUIDIC GENERATOR

I. MASS FLOW CALCULATION THROUGH THE FLUIDIC GENERATOR

It is desirable to know the relationship between the absolute total pressure p_o, the absolute cavity pressure p_c, and the absolute skin pressure just outside the exit hole p_s. To obtain these relationships, assume ideal isentropic flow of air through a nozzle and multiply the mass flow rate expression by C_v, the velocity coefficient:

$$\dot{m} = C_v A_2 \sqrt{\frac{2\gamma}{\gamma-1} \frac{p_{1\rho 1} (p_2/p_o)^{2/\gamma} [1-(p_2/p_o)^{(\gamma-1)/\gamma}]}{[1-(p_2/p_1)^{2/\gamma} (A_2/A_1)^2]}}$$

If state (0) is the stagnation condition, then for $A_2 \ll A_1$, the mass flow rate simplifies for air to

$$\dot{m} = C_v A_2 \sqrt{7\, p_o \rho_o \left(\frac{p_2}{p_o}\right)^{\frac{10}{7}} \left[1-\left(\frac{p_2}{p_o}\right)^{\frac{2}{7}}\right]}$$

Assuming the ideal gas relationship $p_o = \rho_o R T_o$ where R is the gas constant,

$$\dot{m} = C_v A \sqrt{\frac{7\, p_o^2}{R T_o} \left(\frac{p}{p_o}\right)^{5/7} \left[1-\left(\frac{p}{p_o}\right)^{2/7}\right]}$$

$$\dot{m} = \{2.0546\, C_v A p_o/\sqrt{T_o}\} \sqrt{\left(\frac{p}{p_o}\right)^{5/7} \left[1-\left(\frac{p}{p_c}\right)^{2/7}\right]}$$

where $A \sim in^2$, $P_o \sim$ Psia, $T \sim {}^oR$, $\dot{m} \sim$ lbm/sec.

C_v is usually assumed a function of the Reynolds number of the orifice or nozzle. This implies that the mass flow rate from a high pressure to a low pressure through some arbitrary small opening is a function of the dimensionless quantities γ = ratio of specific heats; $R_e = \frac{\dot{m}d}{A\mu}$; p/p_o. The mass flow rate will also depend on the stagnation pressure and temperature, P_o and T_o.

The converging section of the bench setup allows for a smooth, gradual convergence of the air just before it flows into the generator. The mass flow rate was calculated from the pressure ratio relative to this section, assuming that flow through this section is isentropic. This approximation should give an error in the range of ±5%, where the positive error indicates that the mass flow rates calculated are greater than the actual mass flow rates. A simple procedure to get the actual flow rate is to calibrate our setup using a flowmeter and obtaining the relationship of C_V vs Reynolds number. The equation presently used to calculate the mass flow rate is

$$\dot{m} = 0.40324 \frac{p_o}{\sqrt{T_o}} \sqrt{\left(\frac{p_3}{p_o}\right)^{5/7} \left[1-\left(\frac{p_3}{p_o}\right)^{2/7}\right]}$$

II. VELOCITY COEFFICIENT CALCULATIONS

There are two velocity coefficients: C_{VJ}, the expansion from the ram pressure to the cavity, and C_{VH}, the expansion from the cavity through the exit holes to the atmosphere. Each of these coefficients is a measure of the effective area that is reduced by the influence of the boundary layer at the edge of each orifice.

In the present investigation, C_V was studied as a function of Re only. The equation used to calculate C_{VJ} for the expansion from $p_o \rightarrow p_c$ is

$$C_{VJ} = \frac{\dot{m}\sqrt{T_o}}{2.0546\, A_J\, p_o \sqrt{\left(\frac{p_c}{p_o}\right)^{5/7} \left[1-\left(\frac{p_c}{p_o}\right)^{2/7}\right]}}$$

Similarly,

$$C_{VH} = \frac{\dot{m}\sqrt{T_o}}{2.0546\, A_H\, p_o \sqrt{\left(\frac{p_s}{p_c}\right)^{5/7} \left[1-\left(\frac{p_s}{p_c}\right)^{2/7}\right]}}$$

The variables used to calculate C_{vJ} and C_{vH} are described and their origins are noted in the table below.

Variable	Description	Origin
P_o, T_o	Stagnation conditions	Experiment measurement
$\dot{m}$	Mass flow rate	Calculated from smooth converging section
A_J, A_H	Cross-sectional areas	Drawings
P_s	Skin pressure	Experiment measurement
P_c	Cavity pressure	Experiment measurement

APPENDIX C

DERIVATION OF THE EQUATIONS OF FLUIDIC GENERATOR OPERATION

DERIVATION OF EQUATIONS OF FLUID GENERATOR OPERATION

The operation of the fluidic generator has been divided into five components consisting of the annular jet, the jet layer, the resonance tube, the cavity, and the holes (see Figures 1 and 7). A linear differential equation has been written for each of these five components that relate the mass flow and pressure fluctuations in different parts of the generator.

Because of the linearity of the equation we look for solution of the form

$$p' = \hat{p} \exp(\sigma + i\omega)t$$

$$\dot{m}' = \hat{\dot{m}} \exp(\sigma + i\omega)t \qquad (C.1)$$

where ω is the frequency of oscillations, σ the damping coefficient and $\hat{p}$ and $\hat{m}$ are the amplitude of the oscillations. A positive value of σ indicates exponential growth at a particular frequency ω. From the homogeneous system of equations, the amplitude ratios can be obtained. These ratios contain a phase factor giving the phase differences between the various pressures and mass flow through the fluidic generator.

The outcome of the system of these equations is a function $\sigma = \sigma(\omega)$ which gives the damping or growth of acoustical waves of a given frequency and amplitude, and the phase relationship between pressures and mass flow at various locations.

A. Annular Jet

The annular jet is a convergent nozzle; the relation between mass flow and pressure ratio (total pressure before the contraction divided by the static pressure at the exit) is well known. In this analysis we have assumed that the exit pressure equals the cavity pressure, thus

$$\dot{m}_J = C_{v_J} A_J \sqrt{\frac{2\gamma}{\gamma-1} \rho_o \rho_o (p_c/p_o)^{2/\gamma} [1-(p_c/p_o)^{(\gamma-1)/\gamma}]} \text{ for } (p_c/p_o) > \left(\frac{2}{\gamma+1}\right)^{\frac{\gamma}{\gamma-1}}$$

$$= C_{v_J} A_J \sqrt{\frac{2\gamma}{\gamma-1} \rho_o \rho_o \frac{2}{\gamma+1}^{2/(\gamma-1)} \frac{\gamma-1}{\gamma+1}} \text{ for } p_c/p_o < \left(\frac{2}{\gamma+1}\right)^{\frac{\gamma}{\gamma-1}}$$

where p_o, p_c are the total and cavity pressures respectively. The second equation corresponds to shock conditions at the exit. The mass flow coefficient C_{v_J} incorporates possible viscous effects. Typical values of these coefficients are given in Table 1 to 4.

Acoustical fluctuations in the cavity induce fluctuations of the mass flow which are given by the relationship.

$$\dot{m}'_J = \frac{d\dot{m}_J}{dp_c} \quad p'_c$$

where $(\,)'$ denotes acoustical fluctuations and the derivative $\frac{d\dot{m}_J}{dp_c}$ is to be evaluated at the operating point

$$\left(\frac{d\dot{m}_J}{dp_c}\right)_W = \frac{\dot{m}}{\gamma p_c} \frac{1 - \frac{\gamma+1}{2}\left(\frac{p_c}{p_o}\right)^{\frac{\gamma+1}{\gamma}}}{1 - \left(\frac{p_c}{p_o}\right)^{\frac{\gamma-1}{\gamma}}} \text{ for } \frac{pc}{p_o} > \left(\frac{2}{\gamma+1}\right)^{\gamma/(\gamma-1)}$$

$$= 0 \quad \text{for} \quad \frac{pc}{p_o} < \left(\frac{2}{\gamma+1}\right)^{\gamma/(\gamma-1)}$$

The previous relation does not take into consideration the inertial effects on the relationship between the acoustical pressure and mass flow. In order to incorporate these effects, an inertial term was incorporated into the equations. It is assumed that the fluctuating pressure is in part utilized to accelerate the mass flow through the nozzle. The resulting equation is

$$I_J \frac{d\dot{m}_J'}{dt} + \dot{m}_J' \left(\frac{dp_c}{d\dot{m}_J}\right)_w = p_c'$$

From dimensional considerations I_J will be a function of the operating conditions and the geometry of the jet nozzle.

$$I_J = \frac{h}{A_J} f_J (M_J, \text{geometry})$$

where h is the width of the ring jet, A_J its area and f_J varies from a value of order one at $M_J = 0$ to zero at $M_J = 1$. For the purpose of this analysis

$$f_J(M_J) = \begin{cases} 1 \text{ for } M_J < 1 \\ 0 \text{ for } M_J > 1 \end{cases}$$

Seeking a solution as indicated in equation (C.1), the equation for annular jet mass flow can be written as

$$\left[I_J (\sigma+i\omega) + \left(\frac{dp_c}{d\dot{m}_J}\right)_w\right] \hat{\dot{m}}_J = \hat{p}_c$$

B. Jet Layer

The jet layer is the region of interaction between the entering ram-jet and the lip of the resonant tube. In first approximation, the pressure inside and outside the ring jet layer can be considered uniform since the acoustical wavelength is much longer than the distance between the jet exit and the tube lip. The pressure inside (p_T) and outside (p_c) need not be the same instantaneously. Phase differences in their oscillations, however, will

result in a deflection force on the jet layer which will cause a radial displacement and therefore an oscillating mass flow into the tube ($\dot{m}_T$).

Detailed analysis of this interaction is an extremely complex problem and is beyond the scope of current research. A phenomenological model was therefore developed in which the inertia and the curvature effects of the jet layer have been incorporated. The present model assumes curved streamlines with constant radius of curvature as sketched. Furthermore, the jet width is assumed small compared with the radius of curvature of the layer and the ring jet.

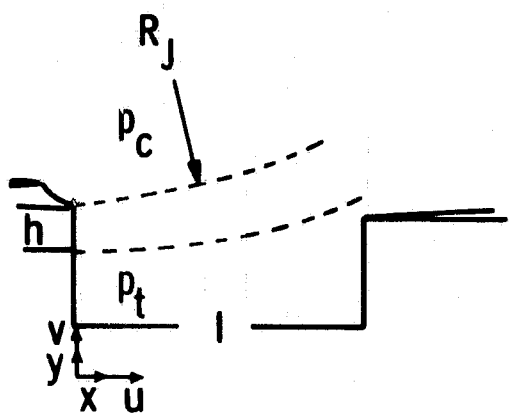

Momentum conservation requires that the pressure differential be balanced by the inertia and the centrifugal force. The inertia term is given by

$$I_J = \int_V \rho \frac{\partial v}{\partial t} dV$$

where

$$v = q \frac{x}{R_J}$$

we find

$$I_J = \rho h W \int_0^{\ell} q \times \frac{\partial}{\partial t}\left(\frac{1}{R_J}\right) dx = \rho h W q \frac{\ell^2}{2} \frac{d(1/R_J)}{dt}$$

where h is the jet width, W its perimeter, and q the jet exit velocity assumed

constant and independent of x. The centrifugal term is given by

$$\rho \frac{q^2}{R_J} \ell W h$$

and finally the pressure force is $(P_T - P_C)\, \ell W$.

Thus

$$\rho\, h\, q \frac{\ell}{2} \frac{d\left(\frac{1}{R_J}\right)}{dt} + \rho \frac{q^2}{R_J} h = (P_T - P_C)$$

The radius of curvature is related with the tube mass flow $\dot{m}'_J$ by the equation

$$1/R_J = -\frac{2}{\ell^2} \frac{\dot{m}'_T}{\rho q W}$$

The relation between the tube mass flow, the pressure in the cavity and the tube is

$$\frac{h}{\ell W} \frac{d\,\dot{m}'_T}{dt} + \frac{2(\dot{m})_W}{\rho \ell^2 W^2} \dot{m}'_T = p'_c - p'_T$$

where $(\dot{m})_W$ is the mass flow through the system at the operating conditions.

For sinusoidal solution we find:

$$\left[\frac{h}{\ell W} (\sigma + i\omega) + \frac{2(\dot{m})_W}{\rho \ell^2 W^2}\right] \hat{\dot{m}}_T = \hat{p}_C - \hat{p}_T$$

C. Resonant Tube

The most important aspect of the operation of the fluidic generator is the energy transfer in the resonant tube. An adequate model of the system has to incorporate its two functions as a) the resonant tube system and b) the "acoustical transmission line" phenomenon through which the energy is transferred to the diaphragm. Depending upon the acoustical wavelength, a variety of tube resonant modes can be excited. At low frequencies, i.e. the wavelength is much longer than the diameter of the tube, only the longitudinal modes are excited. These modes are characterized by plane waves moving back

and forth through the tube. The difference in energy carried by the waves travelling in one direction compared to those moving in the opposite direction is the amount of energy transferred through the tube. The resonant characteristics of the tube are determined by the matching conditions at both ends which in turn determine the amount of energy transmitted.

In the present model, the relationship between the pressure and the mass flow at the entrance of the tube is a function of the amount of energy transferred through the tube.

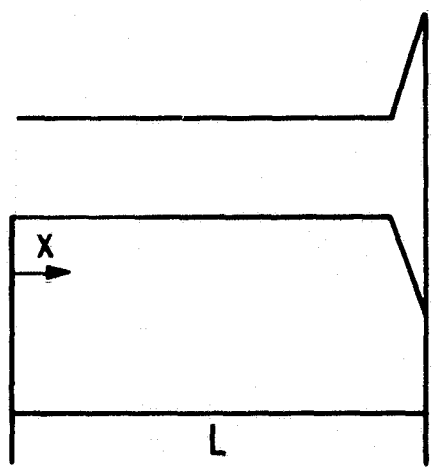

We consider the superposition of right and left propagating acoustical waves. Their amplitude and phase at the diaphragm end are related by the reflexion coefficient $R(\omega)$ which in general is a complex function of the frequency.

In general, if the pressure field associated with the right propagating wave at x=o is

$$p_R = p_R(t)$$

then at any x

$$p_R(t,x) = p_R\ (t - \frac{x}{a})$$

where a is the speed of sound. Similarly for the left propagating wave

$$p_L(t,x) = p_L(t + \frac{x}{a})$$

At the diaphragm end, the reflexion coefficient R is defined as

$$R = \frac{p_L(t + L/a)}{p_R(t - L/a)}$$

For wave forms given by

$$p_R(t) = \hat{p}_R \exp[(\sigma+i\omega)t]$$

$$p_L(t) = \hat{p}_L \exp[(\sigma+i\omega)t]$$

we find

$$R = \frac{p_L}{p_R} \exp\ [2(\sigma+i\omega)\ L/a]$$

and consequently at x=o the pressure fluctuation is given by

$$p_T = (\hat{p}_R + \hat{p}_L) \exp[(\sigma+i\omega)t] = \hat{p}_R \exp[(\sigma+i\omega)t]\ [1+R \exp\ \{-2(\sigma+i\omega)L/ao\}]$$

Associated with the right and left propagating waves there is an acoustical velocity field given by

$$U_R = p_R/\rho a$$

$$U_L = -\ p_L/\rho a$$

Therefore, the velocity at the entrance of the tube is given by

$$U_T = \frac{\hat{p}_R}{\rho a} \exp[(\sigma+i\omega)t]\ \{1-R \exp(-2(\sigma+i\omega)\ L/a)\}$$

The mass flow $\dot{m}'_T = \rho\ U_T\ A_T$ is

$$\dot{m}'_T = \hat{\dot{m}}_T \exp[(\sigma+i\omega)t]$$

$$\hat{\dot{m}}_T = \frac{\hat{p}_R}{a} A_T\ \{1-R \exp\ [-2(\sigma+i\omega)L/a]\}$$

The relationship between $\hat{m}_T$ and $\hat{p}_T$ is

$$\frac{\hat{m}_T}{p_T} = \frac{A_T}{a} \frac{1 - R \exp[-2(\sigma+i\omega) L/a]}{1 + R \exp[-2(\sigma+i\omega) L/a]}$$

The reflection coefficient R is determined by the interaction of the acoustical field with the diaphragm. The diaphragm can be modelled as a second order mechanical system. If x_D is its position then its motion is described by the equation $p'_D A_D = m_D \frac{d^2x_D}{dt2} + f_D \frac{dx_D}{dt} + k_D x_D$

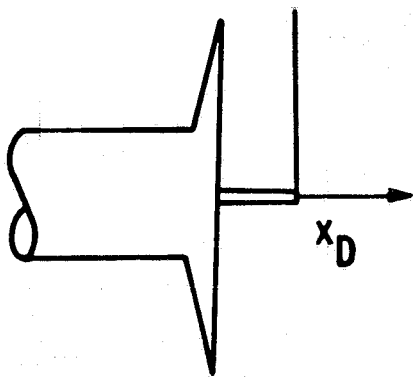

where m_D and k_D are the mass and spring constant of the diaphragm-reed combination, and f_D is the friction coefficient which also incorporates the effects of the energy transmitted into the electrical part of the system. The fluid velocity at the diaphragm is $\frac{dx_D}{dt}$ which results in a velocity at the end of the tube U'_E,

$$U'_E = \frac{A_D}{A_T} U'_D = \frac{A_D}{A_T} \frac{dx_D}{dt}$$

Since p'_E at the end of the tube equals p'_D, we find

$$p'_E/U'_E = A_T/A_D \frac{m_D \frac{d^2x_D}{dt} + f_D \frac{dx_D}{dt} + k_D x_D}{A_D \frac{dx_D}{dt}}$$

The tube equation is given by

$$\frac{p'_E}{U'_E} = \rho a \frac{1+R}{1-R}$$

The reflection coefficient can be written as:

$$R = \frac{(1 - \frac{\rho a A_D^2}{A_T f_D}) \frac{dx_D}{dt} + m_D \frac{d^2x_D}{dt^2} + k_D x_D}{(1 + \frac{\rho a A_D^2}{A_T f_D}) \frac{dx_D}{dt} + m_D \frac{d^2x_D}{dt^2} + k_D x_D}$$

For sinusoidal oscillations, one can write

$$R = \frac{(1 - \frac{\rho a A_D^2}{A_T f_D}) z + m_D z^2 + k_D}{(1 + \frac{\rho a A_D^2}{A_T f_D}) z + m_D z^2 + k_D}$$

where $z = \sigma + i\omega$

Introducing the nondimensional parameters

$$\phi = \frac{\rho a A_D^2}{A_T f_D}$$

$$\eta = \frac{m_D}{f_D} \frac{a}{L}$$

$$\Omega = \sqrt{\frac{k_D}{m} \frac{L}{a}}$$

The term coefficient can be written as

$$R = \frac{1 - \phi + \eta \frac{Lz}{a} \left[1 + (\frac{\Omega}{Lz/a})^2\right]}{1 + \phi + \eta \frac{Lz}{a} \left[1 + (\frac{\Omega}{Lz/a})^2\right]}$$

D. Cavity

Both the jet and the tube are located inside a cavity which plays a role in the acoustical properties of the system. For the frequencies of fluidic generator operation, this cavity is operating as an accumulator because the wavelength is very large compared with the characteristic dimension of the cavity. The acoustical pressure inside the cavity can also be considered uniform. Furthermore, the characteristic time of the oscillations is short enough to neglect the heat transfer from the fluid to the wall. Therefore the cavity can be modeled as an isentropic accumulator for which the relation between the mass flow and cavity pressure is given by

$$\frac{dp_c'}{dt} = \frac{\gamma R T_c}{V_c} \dot{m}_c'$$

where γ is the ratio of specific heats, R the gas constant, T_c the gas temperature and V_c the cavity volume.

This equation gives for oscillatory waves

$$(\sigma+i\omega)\ \hat{p}_c = \frac{\gamma R T_c}{V_c}\ \hat{\dot{m}}_c$$

E. Holes

The equation modeling the behavior of the exit holes is identical to that governing the behavior of the annular jet. It should be noted that for the exit holes, the acoustical fluctuations depend on the total pressure upstream of the orifice rather than at the exit pressure; thus:

$$\dot{m}_H = C_{v_H} A_H \sqrt{\frac{2\gamma}{\gamma-1} p_c \rho_c \left(\frac{p_s}{p_c}\right)^{2/\gamma} \left[1-\left(\frac{p_s}{p_c}\right)^{\frac{\gamma-1}{\gamma}}\right]} \; ; \; \frac{p_s}{p_c} > \left(\frac{2}{\gamma+1}\right)^{\gamma/\gamma-1}$$

$$= C_{v_H} A_H \sqrt{\gamma \left(\frac{2}{\gamma+1}\right)^{\frac{\gamma+1}{\gamma-1}} p_c \rho_c} \; ; \; \frac{p_s}{p_c} < \left(\frac{2}{\gamma+1}\right)^{\gamma/\gamma-1}$$

Therefore the linearized equation is

$$I_H \frac{d \dot{m}_H'}{dt} + \left(\frac{dp_c}{d\dot{m}_H}\right)_w \dot{m}_H' = p_c'$$

with

$$\left(\frac{dp_c}{d\dot{m}_H}\right)_w^{-1} = \left(\frac{d\dot{m}_H}{dp_c}\right)_w = \begin{cases} \dfrac{\dot{m}(\gamma-1)p_c}{2\gamma} \dfrac{2-(p_s/p_c)^{\gamma-1/\gamma}}{1-(p_s/p_c)^{\gamma-1}} & ; \; p_s/p_c > \left(\dfrac{2}{\gamma+1}\right)^{\gamma/\gamma-1} \\ \dfrac{\dot{m}}{p_c} & ; \; p_s/p_c < \left(\dfrac{2}{\gamma+1}\right)^{\gamma/\gamma-1} \end{cases}$$

$$I_H = \frac{4}{\pi d_H} f_H \; (M_{ex}, \text{geometry}); \; f_H \; (M_{ex}, \text{geometry}) = 1$$

f_H has been assumed independent of the exit Mach number.

Thus for sinusoidal oscillations, we find

$$\left[I_H \; (\sigma+i\omega) + \left(\frac{dp_c}{d\dot{m}_H}\right)\right]_w \hat{\dot{m}}_H = \hat{p}_c$$

APPENDIX D

COMPUTER PROGRAM FOR MODELING THE FLUIDIC POWER GENERATOR

```
PAGE  0001          FTN4 COMPILER: HP24177  (SEPT, 1974)

0001  FTN4,L
0002        PROGRAM PLGEN
0003        COMPLEX R,P,Z(101),ZX
0004        REAL MS
0005        COMMON AJ,BJ,AH,BH,AT,BT,XK,ET,UM,PHI,R,M
0006        DIMENSION P(101)
0007        EXTERNAL ACURE
0008        DATA C1/.6V6P1M736/,EX/.285714/,C2/.8333333/
0009        AJ=.5243
0010        AH=.69565
0011        AT=.71322
0012        XK=14.5831
0013      5 WRITE(1,100)
0014    100 FORMAT("E/P0,PC,PS,MS,ET,UME,M,ERR,N")
0015        READ(1,*)P0,PC,PS,MS,ET,UM,M,ERR,N
0016        IF(P0.LE.0.)STOP
0017        PR=(PC/P0)**EX
0018        IF(PR.LE.C2)GO TO 1
0019        BJ=C1*PC/MS*7.*(1.-PR)/(5.-6.*PR)
0020      6 PR=(PS/PC)**EX
0021        AUX=7.*(1.-PR)/(2.-PR)
0022        IF(PR.LE.C2)AUX=1.
0023        BH=C1*PC/MS*AUX
0024        BT=3.4993*MS
0025        ZX=CMPLX(0.,P)
0026        DO 2 J=1,101
0027        PHI=(J-1)*.01
0028      7 NI=N
0029        CALL NEWCO(ACURE,ZX,ERR,NI)
0030        IF(NI.LT.0)GO TO 3
0031        Z(J)=ZX
0032        P(J)=PHI
0033      2 CONTINUE
0034        WRITE(6,200)AJ,BJ,AH,BH,AT,BT,XK,ET,UM
0035    200 FORMAT(1H1,2X,"AJ =",E9.4,2X,"BJ =",E9.4,2X,"AH =",E9.4,2X,"BH =",
0036       1E9.4,2X,"AT =",E9.4/10X,"BT =",E9.4,2X,"K =",E9.4,2X,"ET =",E9.4,
0037       22X,"UM =",E9.4//1H0,5X,"PHI",7X,"REAL",7X,"IMAG")
0038        WRITE(6,201)(P(J),Z(J),J=1,101)
0039    201 FORMAT(3X,E9.4,1X,E16.4,2X,E9.4)
0040        GO TO 5
0041      1 BJ=1.
0042        GO TO 6
0043      3 WRITE(1,101)PHI
0044    101 FORMAT("NEWCO DIDN'T CONVERGE PHI =",E9.4/"E/1 N TIMES MORE,2 STAR
0045       1T")
0046        READ(1,*)IC
0047        GO TO (7,5)IC
0048        END

**  NO ERRORS**     PROGRAM = 01145       COMMON = 00028
```

```
        PAGE  0001          FTN4 COMPILER: HP24177  (SEPT, 1974)

0049          SUBROUTINE NEWCO(FUNC,X,ERR,NI)
0050          COMPLEX F,DF,X
0051          DO 1 I=1,NI
0052          CALL FUNC(F,DF,X)
0053          FR=REAL(F)
0054          FI=AIMAG(F)
0055          AUX=SQRT(FR**2+FI**2)
0056          IF(AUX.LE.ERR)GO TO 2
0057        1 X=X-F/DF
0058          NI=-1
0059        2 RETURN
0060          END

**  NO ERRORS**     PROGRAM = 00101       COMMON = 00000


        PAGE  0001          FTN4 COMPILER: HP24177  (SEPT, 1974)

0001          SUBROUTINE ACORE(F,DF,X)
0002          COMPLEX F,DF,X,R,M,XJ,XH,XT,AUX,AUX1,AUX2,DM,DR
0003          COMMON AJ,BJ,AH,BH,AT,BT,XK,ET,OM,PHI,R,M
0004          AUX=CEXP(X)
0005          AUX1=1.+PHI+ET*X*(1.+OM**2/X**2)
0006          R=(AUX1-2.*PHI)/AUX1
0007          AUX2=AUX-R/AUX
0008          M=(AUX+R/AUX)/AUX2
0009          XJ=1./(AJ*X+BJ)
0070          IF(BJ.GT.0.)XJ=(0.,0.)
0071          XH=AH*X+BH
0072          XT=AT*X+BT+M
0073          AUX=XK*X+XJ+1./XH
0074          F=XT*AUX+(1.,0.)
0075          DR=2.*PHI*ET*(1.-OM**2/X**2)/AUX1**2
0076          DM=2.*(DR-2.*R)/AUX2**2+AT
0077          AUX1=XK-AH/XH**2-AJ*XJ**2
0078          DF=DM*AUX+XT*AUX1
0079          RETURN
0080          END

**  NO ERRORS**     PROGRAM = 00506       COMMON = 00028
```

AJ =.5243E+00 BJ =-.376E+01 AH =.9365E-01 BH =.3707E+00 AT =.1322E-01
BT =.9437E-01 K =.1458E+02 ET =.2253E+02 DM =.9460E+00

PHI	REAL	IMAG
.0000E+00	-.9481E-01	.1595E+01
1.000E-02	-.9478E-01	.1595E+01
.2000E-01	-.9475E-01	.1596E+01
.3000E-01	-.9471E-01	.1596E+01
.4000E-01	-.9468E-01	.1596E+01
.5000E-01	-.9465E-01	.1597E+01
.6000E-01	-.9461E-01	.1597E+01
.7000E-01	-.9458E-01	.1598E+01
.8000E-01	-.9455E-01	.1598E+01
.9000E-01	-.9451E-01	.1599E+01
1.000E-01	-.9448E-01	.1599E+01
.1100E+00	-.9445E-01	.1599E+01
.1200E+00	-.9441E-01	.1600E+01
.1300E+00	-.9438E-01	.1600E+01
.1400E+00	-.9435E-01	.1601E+01
.1500E+00	-.9432E-01	.1601E+01
.1600E+00	-.9428E-01	.1601E+01
.1700E+00	-.9425E-01	.1602E+01
.1800E+00	-.9422E-01	.1602E+01
.1900E+00	-.9419E-01	.1603E+01
.2000E+00	-.9416E-01	.1603E+01
.2100E+00	-.9413E-01	.1603E+01
.2200E+00	-.9409E-01	.1604E+01
.2300E+00	-.9406E-01	.1604E+01
.2400E+00	-.9403E-01	.1605E+01
.2500E+00	-.9400E-01	.1605E+01
.2600E+00	-.9397E-01	.1605E+01
.2700E+00	-.9394E-01	.1606E+01
.2800E+00	-.9391E-01	.1606E+01
.2900E+00	-.9388E-01	.1607E+01
.3000E+00	-.9384E-01	.1607E+01
.3100E+00	-.9381E-01	.1607E+01
.3200E+00	-.9378E-01	.1608E+01
.3300E+00	-.9375E-01	.1608E+01
.3400E+00	-.9372E-01	.1609E+01
.3500E+00	-.9369E-01	.1609E+01
.3600E+00	-.9366E-01	.1609E+01
.3700E+00	-.9363E-01	.1610E+01
.3800E+00	-.9360E-01	.1610E+01
.3900E+00	-.9357E-01	.1610E+01
.4000E+00	-.9354E-01	.1611E+01
.4100E+00	-.9351E-01	.1611E+01
.4200E+00	-.9348E-01	.1612E+01
.4300E+00	-.9345E-01	.1612E+01
.4400E+00	-.9343E-01	.1612E+01
.4500E+00	-.9340E-01	.1613E+01
.4600E+00	-.9337E-01	.1613E+01
.4700E+00	-.9334E-01	.1614E+01
.4800E+00	-.9331E-01	.1614E+01
.4900E+00	-.9328E-01	.1614E+01
.5000E+00	-.9325E-01	.1615E+01
.5100E+00	-.9322E-01	.1615E+01
.5200E+00	-.9319E-01	.1616E+01
.5300E+00	-.9317E-01	.1616E+01
.5400E+00	-.9314E-01	.1616E+01
.5500E+00	-.9311E-01	.1617E+01

Table 1. Data for All Exit Holes, Open Area

- ALL EXIT HOLES OPEN , PS=14.32PSI

P0	PC	P3	M	PC/P0	PINF/PC	C_{VJ}	C_{VH}	PC/P0	MSFL/P0 (FT*S)
14.932	14.409	14.881	0.0000813	0.96496	0.99389	0.91799E+00	0.66736E+00	0.9649551E+00	0.1168119E-06
15.544	14.487	15.442	0.0116407	0.93200	0.96854	0.92918E+00	0.70537E+00	0.9319951E+00	0.1616402E-06
16.187	14.575	16.036	0.0144378	0.90043	0.98257	0.93159E+00	0.70225E+00	0.9004269E+00	0.1925888E-06
16.767	14.653	16.575	0.0165719	0.87391	0.97734	0.93234E+00	0.70532E+00	0.8739113E+00	0.2133286E-06
17.344	14.727	17.118	0.0185633	0.84914	0.97240	0.93751E+00	0.71412E+00	0.8491402E+00	0.2318149E-06
17.959	14.809	17.685	0.0204872	0.82459	0.96786	0.93786E+00	0.71688E+00	0.8245856E+00	0.2452648E-06
19.158	14.971	18.811	0.0237859	0.78148	0.95655	0.94215E+00	0.72148E+00	0.7814773E+00	0.2670815E-06
20.380	15.147	19.966	0.0267830	0.74323	0.94543	0.94588E+00	0.72116E+00	0.7432345E+00	0.2827989E-06
21.617	15.327	21.128	0.0295208	0.70902	0.93435	0.95033E+00	0.72295E+00	0.7090238E+00	0.2947561E-06
22.836	15.518	22.297	0.0321706	0.67918	0.92333	0.95597E+00	0.72504E+00	0.6791846E+00	0.3040660E-06
24.076	15.703	23.482	0.0346464	0.65223	0.91198	0.95909E+00	0.72465E+00	0.6522329E+00	0.3105751E-06
25.375	15.903	24.724	0.0372841	0.62673	0.90052	0.96423E+00	0.72764E+00	0.6267253E+00	0.3164626E-06
26.559	16.093	25.863	0.0393516	0.60593	0.88998	0.96627E+00	0.72762E+00	0.6059293E+00	0.3198078E-06
27.823	16.289	27.061	0.0415564	0.58545	0.87917	0.96888E+00	0.72938E+00	0.5854638E+00	0.3223823E-06
29.045	16.486	28.258	0.0437269	0.56759	0.86869	0.97193E+00	0.73216E+00	0.5675927E+00	0.3249488E-06
30.288	16.682	29.469	0.0453881	0.55078	0.85846	0.97418E+00	0.73478E+00	0.5507847E+00	0.3264414E-06
31.531	16.879	30.661	0.0478892	0.53530	0.84846	0.97739E+00	0.73842E+00	0.5353828E+00	0.3278174E-06
32.781	17.082	31.870	0.0499747	0.52189	0.83837	0.98087E+00	0.74285E+00	0.5218927E+00	0.3298584E-06
34.038	17.292	33.085	0.0520649	0.50883	0.82818	0.98417E+00	0.74565E+00	0.5089252E+00	0.3301563E-06
35.318	17.505	34.323	0.0542234	0.49564	0.81889	0.98788E+00	0.75048E+00	0.4955420E+00	0.3313734E-06
36.568	17.719	35.533	0.0562571	0.48454	0.80823	0.98982E+00	0.75418E+00	0.4845425E+00	0.3320537E-06
37.672	17.775	36.593	0.0582736	0.47187	0.80562	0.99525E+00	0.77478E+00	0.4718690E+00	0.3338745E-06
39.098	18.166	37.978	0.0604964	0.46463	0.78834	0.99554E+00	0.76324E+00	0.4646265E+00	0.3339704E-06
40.458	18.417	39.294	0.0627168	0.45520	0.77761	0.99737E+00	0.76711E+00	0.4552034E+00	0.3345845E-06
42.519	18.883	41.291	0.0660369	0.44222	0.76164	0.99928E+00	0.77288E+00	0.4422240E+00	0.3352264E-06

Table 2. Data for 7/8 Exit Holes, Open Area

- 7/8 EXIT HOLES OPEN , PS=14.32PSI

P0	PC	P3	M	PC/P0	PINF/PC	C_{VJ}	C_{VH}	PC/P0	MSFL/P0 (FT*S)
14.998	14.443	14.941	0.0005354	0.96301	0.99156	0.94878E+00	0.68464E+00	0.9630141E+00	0.1228384E-06
15.605	14.538	15.588	0.0118763	0.93159	0.98589	0.94161E+00	0.71464E+00	0.9315915E+00	0.1642636E-06
16.247	14.646	16.895	0.0145535	0.90144	0.97779	0.93964E+00	0.71523E+00	0.9014429E+00	0.1933369E-06
16.848	14.744	16.654	0.0166926	0.87514	0.97128	0.93848E+00	0.71910E+00	0.8751388E+00	0.2138493E-06
17.581	14.853	17.263	0.0187958	0.84878	0.96419	0.93964E+00	0.72268E+00	0.8486973E+00	0.2316134E-06
18.157	14.965	17.878	0.0207288	0.82419	0.95699	0.94145E+00	0.72469E+00	0.8241899E+00	0.2464168E-06
19.354	15.168	19.085	0.0238929	0.78378	0.94416	0.94338E+00	0.72858E+00	0.7836958E+00	0.2664560E-06
20.642	15.388	20.221	0.0270561	0.74547	0.93065	0.94884E+00	0.73541E+00	0.7454731E+00	0.2829891E-06
21.888	15.608	21.485	0.0298234	0.71318	0.91752	0.95191E+00	0.73845E+00	0.7131008E+00	0.2940958E-06
23.175	15.849	22.632	0.0325247	0.68387	0.90368	0.95577E+00	0.73968E+00	0.6838742E+00	0.3029193E-06
24.588	16.096	23.899	0.0351748	0.65698	0.88971	0.95958E+00	0.74258E+00	0.6569750E+00	0.3096725E-06
25.791	16.348	25.134	0.0376746	0.63356	0.87643	0.96379E+00	0.74624E+00	0.6335589E+00	0.3152951E-06
27.046	16.588	26.341	0.0399823	0.61384	0.86372	0.96659E+00	0.74906E+00	0.6138368E+00	0.3198722E-06
28.396	16.852	27.641	0.0423559	0.59346	0.84983	0.96884E+00	0.75034E+00	0.5934569E+00	0.3219563E-06
29.731	17.119	28.927	0.0447154	0.57581	0.83654	0.97254E+00	0.75381E+00	0.5758874E+00	0.3246273E-06
31.088	17.383	30.153	0.0468685	0.56576	0.82383	0.97583E+00	0.75576E+00	0.5687686E+00	0.3263381E-06
32.387	17.654	31.415	0.0491086	0.54646	0.81118	0.97857E+00	0.75938E+00	0.5464687E+00	0.3288386E-06
33.662	17.942	32.727	0.0513191	0.53381	0.79816	0.98093E+00	0.76203E+00	0.5338185E+00	0.3299327E-06
34.969	18.224	33.992	0.0534488	0.52113	0.78585	0.98341E+00	0.76586E+00	0.5211319E+00	0.3299327E-06
36.318	18.518	35.286	0.0557549	0.51068	0.77334	0.98795E+00	0.77089E+00	0.5099580E+00	0.3314237E-06
37.655	18.816	36.596	0.0580129	0.49978	0.76189	0.99126E+00	0.77482E+00	0.4997023E+00	0.3325389E-06
39.053	19.135	37.965	0.0604352	0.48959	0.74842	0.99491E+00	0.78063E+00	0.4895943E+00	0.3337590E-06
40.389	19.436	39.229	0.0625625	0.48123	0.73681	0.99662E+00	0.78451E+00	0.4812251E+00	0.3343342E-06

ORIGINAL PAGE IS
OF POOR QUALITY

Table 3. Data for 3/4 Exit Holes, Open Area

- 3/4 EXIT HOLES OPEN , PS=14.32PSI

P0	PC	P3	M	PC/P0	PINF/PC	C_{VJ}	C_{VH}	PC/P0	MSFL/P0 (FT*S)
14.685	14.385	14.582	0.0053335	0.98495	0.99553	0.93493E+00	0.68693E+00	0.9849514E+00	0.7882891E-07
15.035	14.488	14.978	0.0085468	0.96311	0.98980	0.94066E+00	0.69999E+00	0.9631858E+00	0.1226867E-06
15.319	14.534	15.248	0.0101992	0.94876	0.98532	0.94249E+00	0.72167E+00	0.9487606E+00	0.1437818E-06
15.645	14.599	15.542	0.0117857	0.93318	0.96097	0.94169E+00	0.73107E+00	0.9331845E+00	0.1625940E-06
15.975	14.666	15.846	0.0132328	0.91818	0.97644	0.94484E+00	0.73605E+00	0.9181848E+00	0.1787826E-06
16.328	14.738	16.176	0.0145981	0.90257	0.97173	0.94232E+00	0.73928E+00	0.9025728E+00	0.1928616E-06
16.644	14.802	16.478	0.0156897	0.88933	0.96758	0.94822E+00	0.73994E+00	0.8853283E+00	0.2034648E-06
16.962	14.866	16.765	0.0167484	0.87658	0.96331	0.94803E+00	0.74193E+00	0.8765767E+00	0.2131548E-06
17.338	14.944	17.114	0.0178794	0.86231	0.95829	0.93805E+00	0.74102E+00	0.8623092E+00	0.2226769E-06
17.885	15.059	17.632	0.0195892	0.84208	0.95896	0.94176E+00	0.74510E+00	0.8420027E+00	0.2364842E-06
18.287	15.147	18.012	0.0208657	0.82831	0.94543	0.94044E+00	0.74415E+00	0.8283871E+00	0.2439118E-06
18.798	15.253	18.484	0.0220513	0.81173	0.93892	0.94297E+00	0.74815E+00	0.8117348E+00	0.2533829E-06
19.133	15.324	18.809	0.0229197	0.80089	0.93456	0.94282E+00	0.74965E+00	0.8008922E+00	0.2585541E-06
19.771	15.459	19.429	0.0245976	0.78198	0.92637	0.94791E+00	0.75536E+00	0.7819049E+00	0.2685306E-06
20.215	15.557	19.832	0.0255659	0.76961	0.92852	0.94567E+00	0.75347E+00	0.7696257E+00	0.2729761E-06
20.958	15.717	20.529	0.0272615	0.75021	0.91119	0.94760E+00	0.75652E+00	0.7502104E+00	0.2888788E-06
21.667	15.879	21.218	0.0288655	0.73286	0.90186	0.95021E+00	0.75840E+00	0.7328789E+00	0.2875528E-06
22.332	16.032	21.844	0.0303038	0.71787	0.89329	0.95249E+00	0.76018E+00	0.7178726E+00	0.2928856E-06
22.998	16.188	22.472	0.0316707	0.70418	0.88469	0.95427E+00	0.76208E+00	0.7040985E+00	0.2973326E-06
23.676	16.352	23.126	0.0331054	0.69057	0.87589	0.95734E+00	0.76312E+00	0.6905686E+00	0.3017983E-06
24.379	16.528	23.797	0.0345452	0.67763	0.86691	0.96042E+00	0.76534E+00	0.6775991E+00	0.3058410E-06
25.474	16.787	24.846	0.0366427	0.65899	0.85389	0.96265E+00	0.76701E+00	0.6589932E+00	0.3104725E-06
26.458	17.031	25.783	0.0384853	0.64389	0.84087	0.96513E+00	0.76894E+00	0.6438852E+00	0.3140467E-06
27.849	17.383	27.127	0.0410599	0.62419	0.82383	0.96850E+00	0.77243E+00	0.6241927E+00	0.3182258E-06
29.262	17.749	28.487	0.0435063	0.60657	0.80685	0.97160E+00	0.77567E+00	0.6065663E+00	0.3214996E-06
30.681	18.122	29.855	0.0460624	0.59065	0.79825	0.97435E+00	0.77924E+00	0.5906535E+00	0.3248478E-06
32.173	18.525	31.294	0.0486426	0.57588	0.77386	0.97765E+00	0.78321E+00	0.5757998E+00	0.3263333E-06
33.568	18.908	32.632	0.0510382	0.56340	0.75741	0.98115E+00	0.78719E+00	0.5634081E+00	0.3282484E-06
35.117	19.345	34.136	0.0536654	0.55097	0.74829	0.98434E+00	0.79204E+00	0.5508669E+00	0.3298137E-06
36.487	19.741	35.461	0.0559442	0.54105	0.72543	0.98686E+00	0.79568E+00	0.5418527E+00	0.3309416E-06
38.043	20.199	36.964	0.0585688	0.53094	0.70981	0.99056E+00	0.80083E+00	0.5309398E+00	0.3322943E-06
39.489	20.629	38.361	0.0610853	0.52248	0.69422	0.99398E+00	0.80683E+00	0.5223997E+00	0.3334487E-06
41.089	21.118	39.929	0.0636638	0.51375	0.67848	0.99688E+00	0.81174E+00	0.5137536E+00	0.3344218E-06
42.524	21.552	41.294	0.0660983	0.50673	0.66454	0.99996E+00	0.81747E+00	0.5067772E+00	0.3354552E-06

Table 4. Data for 1/2 Exit Holes, Open Area

- 1/2 EXIT HOLES OPEN , PS=14.16PSI

P0	PC	P3	M	PC/P0	PINF/PC	C_{VJ}	C_{VH}	PC/P0	MSFL/P0 (FT*S)
14.458	14.261	14.437	0.0050809	0.98641	0.99266	0.94602E+00	0.77433E+00	0.9864095E+00	0.7565366E-07
14.769	14.366	14.729	0.0070907	0.97270	0.98543	0.91888E+00	0.76432E+00	0.9727038E+00	0.1036270E-06
15.135	14.491	15.073	0.0089913	0.95747	0.97689	0.91857E+00	0.76645E+00	0.9574721E+00	0.1202230E-06
15.686	14.680	15.503	0.0113668	0.93586	0.96435	0.92364E+00	0.77553E+00	0.9358568E+00	0.1564289E-06
16.459	14.952	16.318	0.0141013	0.90841	0.94680	0.92861E+00	0.78090E+00	0.9084097E+00	0.1849172E-06
17.161	15.214	16.982	0.0161893	0.88649	0.93052	0.93068E+00	0.77621E+00	0.8864943E+00	0.2036126E-06
17.867	15.486	17.652	0.0180798	0.86671	0.91417	0.93256E+00	0.77557E+00	0.8667083E+00	0.2184061E-06
18.481	15.726	18.234	0.0196966	0.85097	0.90017	0.93816E+00	0.77792E+00	0.8509681E+00	0.2308423E-06
19.159	15.999	18.888	0.0213027	0.83503	0.88486	0.93984E+00	0.77726E+00	0.8350287E+00	0.2399873E-06
19.807	16.271	19.498	0.0227878	0.82144	0.87086	0.94318E+00	0.77663E+00	0.8214425E+00	0.2483175E-06
20.480	16.511	20.065	0.0240823	0.80936	0.85738	0.94411E+00	0.77814E+00	0.8093628E+00	0.2547947E-06
21.066	16.783	20.781	0.0254785	0.79673	0.84348	0.94452E+00	0.77974E+00	0.7967269E+00	0.2609742E-06
21.652	17.035	21.262	0.0267319	0.78674	0.83104	0.94809E+00	0.78232E+00	0.7867441E+00	0.2664785E-06
22.273	17.296	21.858	0.0279416	0.77656	0.81847	0.94788E+00	0.78343E+00	0.7765658E+00	0.2727749E-06
22.877	17.558	22.437	0.0291332	0.76751	0.80627	0.94934E+00	0.78531E+00	0.7675856E+00	0.2746710E-06
23.476	17.820	23.005	0.0303116	0.75924	0.79443	0.95178E+00	0.78786E+00	0.7592489E+00	0.2787558E-06
24.061	18.092	23.574	0.0314224	0.75192	0.78249	0.95388E+00	0.78853E+00	0.7519153E+00	0.2818775E-06
24.641	18.353	24.132	0.0325221	0.74483	0.77133	0.95460E+00	0.79079E+00	0.7448323E+00	0.2846748E-06
25.197	18.685	24.665	0.0336018	0.73836	0.76092	0.95716E+00	0.79413E+00	0.7383633E+00	0.2878363E-06
25.825	18.898	25.271	0.0347276	0.73174	0.74912	0.95788E+00	0.79555E+00	0.7317434E+00	0.2902411E-06
26.327	19.128	25.753	0.0356483	0.72656	0.74019	0.95918E+00	0.79766E+00	0.7265567E+00	0.2922633E-06
26.945	19.421	26.349	0.0367625	0.72076	0.72893	0.96851E+00	0.80824E+00	0.7207613E+00	0.2944824E-06
27.453	19.662	26.838	0.0376845	0.71618	0.72081	0.96189E+00	0.80265E+00	0.7161834E+00	0.2962784E-06
27.996	19.923	27.361	0.0386854	0.71164	0.71255	0.96408E+00	0.80558E+00	0.7116429E+00	0.2982586E-06
28.597	20.216	27.941	0.0397262	0.70693	0.70425	0.96488E+00	0.80758E+00	0.7069263E+00	0.2998348E-06
29.458	20.635	28.763	0.0412220	0.70068	0.68684	0.96667E+00	0.81129E+00	0.7006835E+00	0.3021265E-06
29.934	20.876	29.231	0.0420661	0.69738	0.67813	0.96769E+00	0.81341E+00	0.6973811E+00	0.3033153E-06
30.725	21.273	29.995	0.0434044	0.69238	0.66546	0.96866E+00	0.81628E+00	0.6923787E+00	0.3049112E-06
31.454	21.648	30.699	0.0446428	0.68798	0.65419	0.96971E+00	0.81947E+00	0.6879821E+00	0.3063392E-06
32.193	22.016	31.412	0.0459484	0.68389	0.64388	0.97185E+00	0.82359E+00	0.6838874E+00	0.3080894E-06

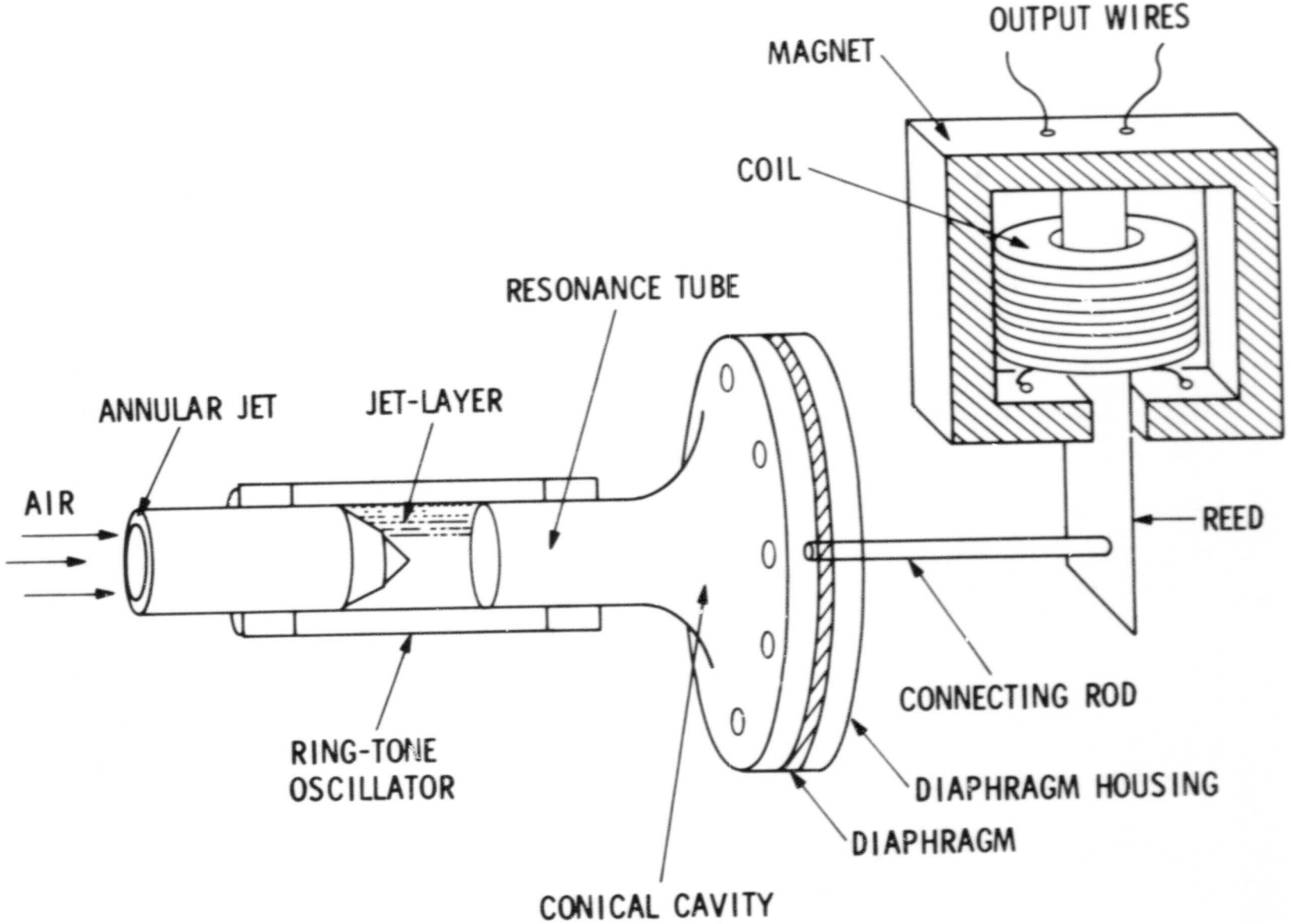

Figure 1. Fluidic Electric Power Generator

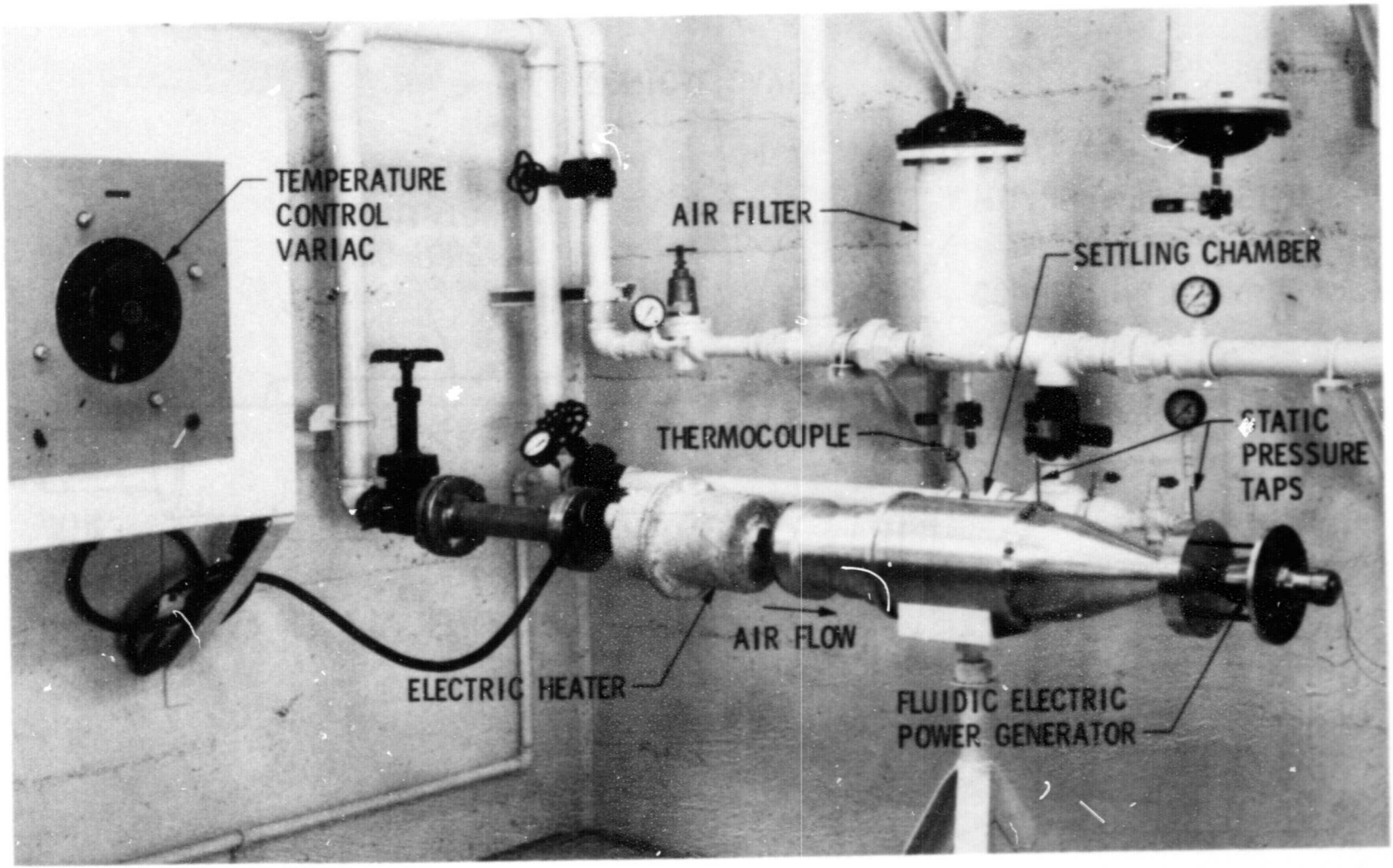

Figure 2. Experimental Setup for Fluidic Generator Bench Test

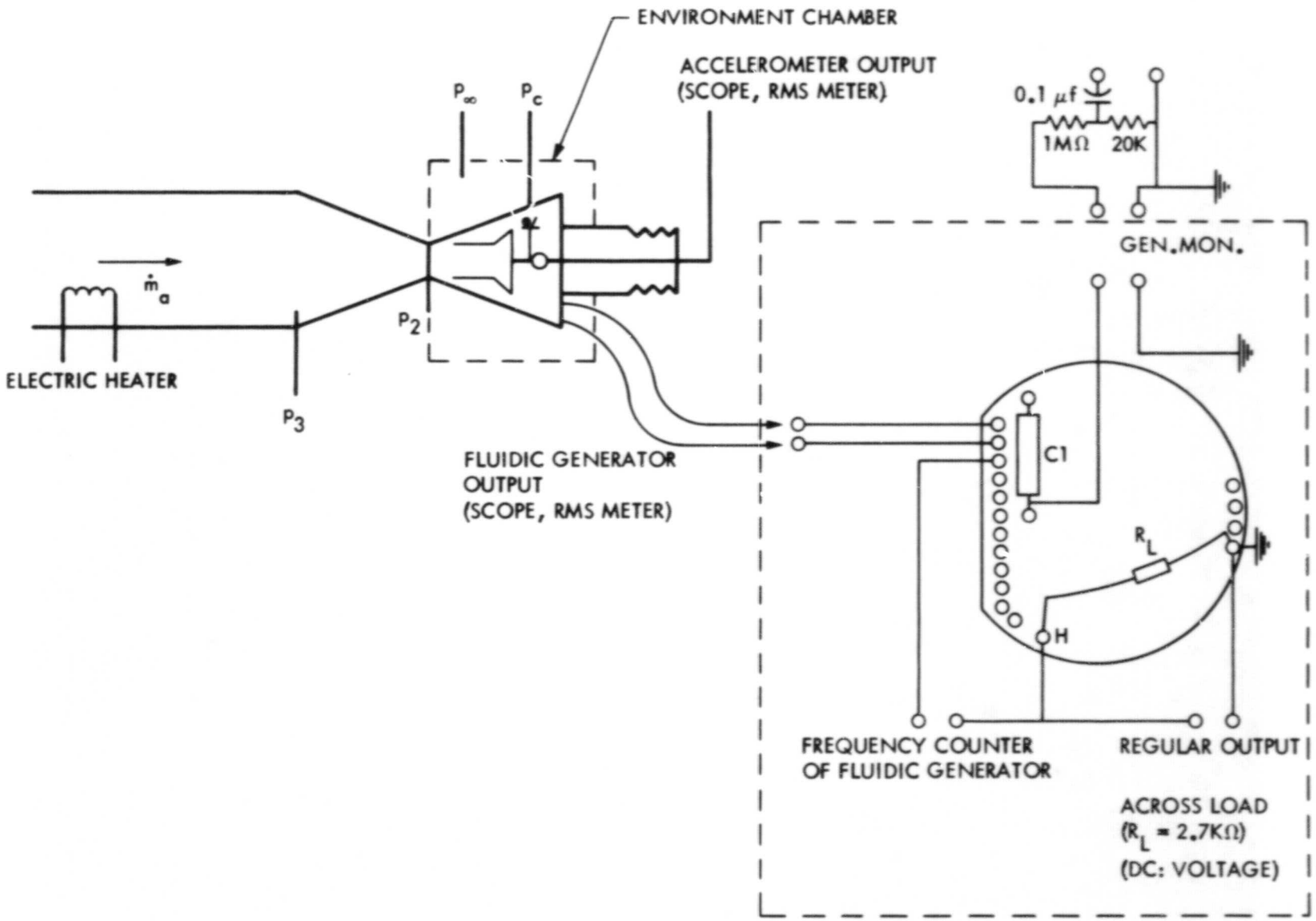

Figure 3. Instrumentation of Fluidic Electric Power Generator

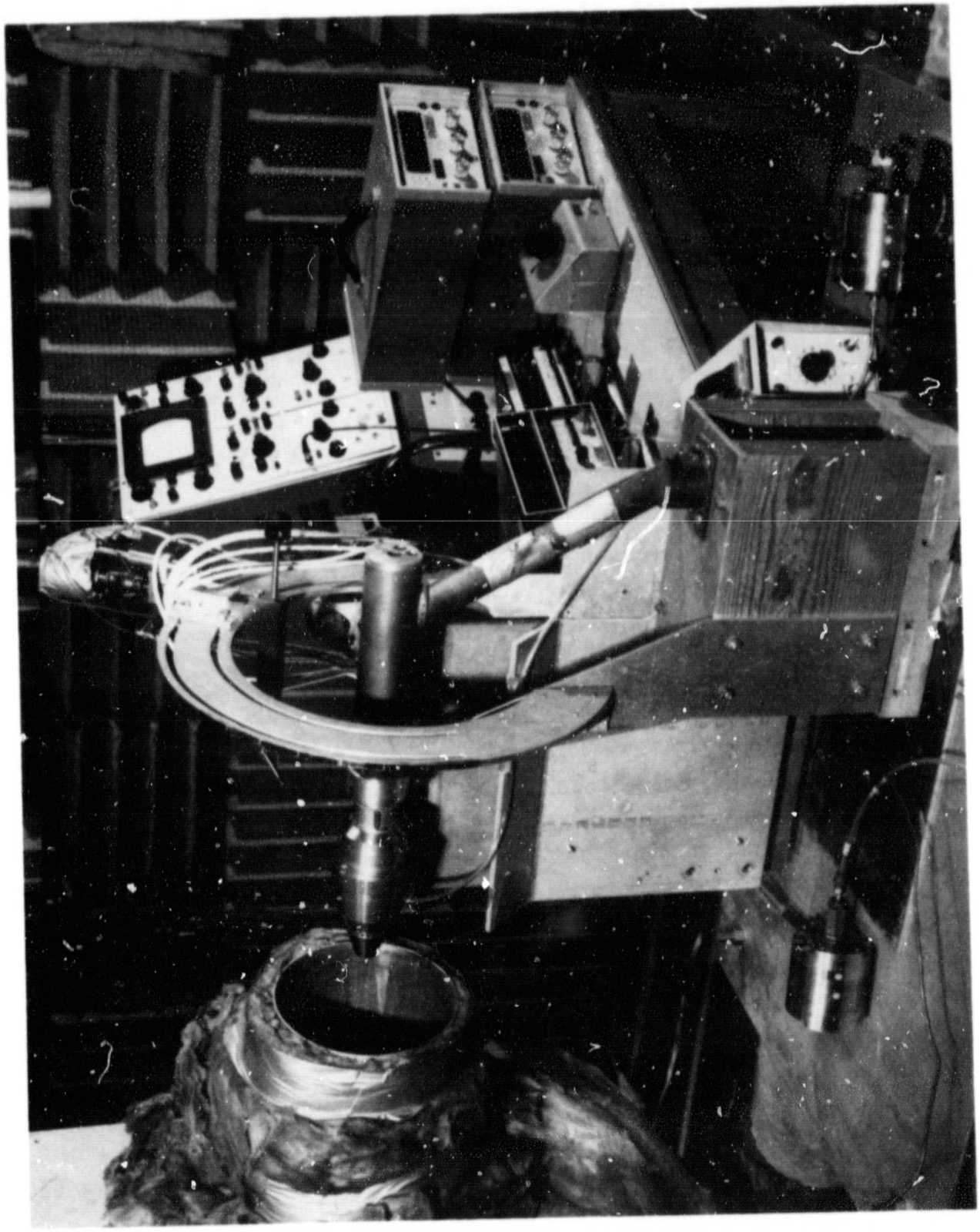

Figure 4. Free-Jet Test Setup

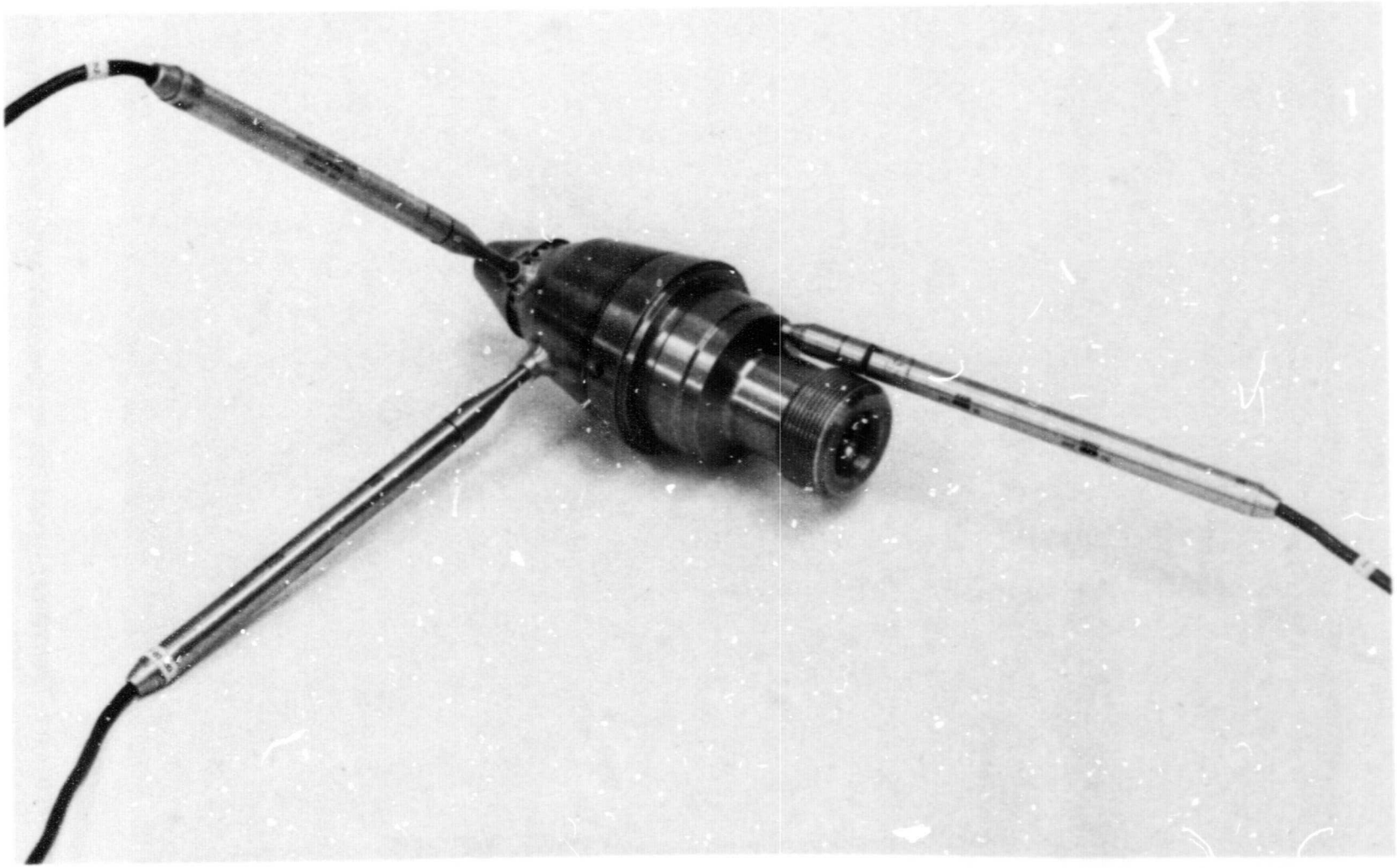

Figure 5. Fluidic Generator Showing the Pressure Transducer Location

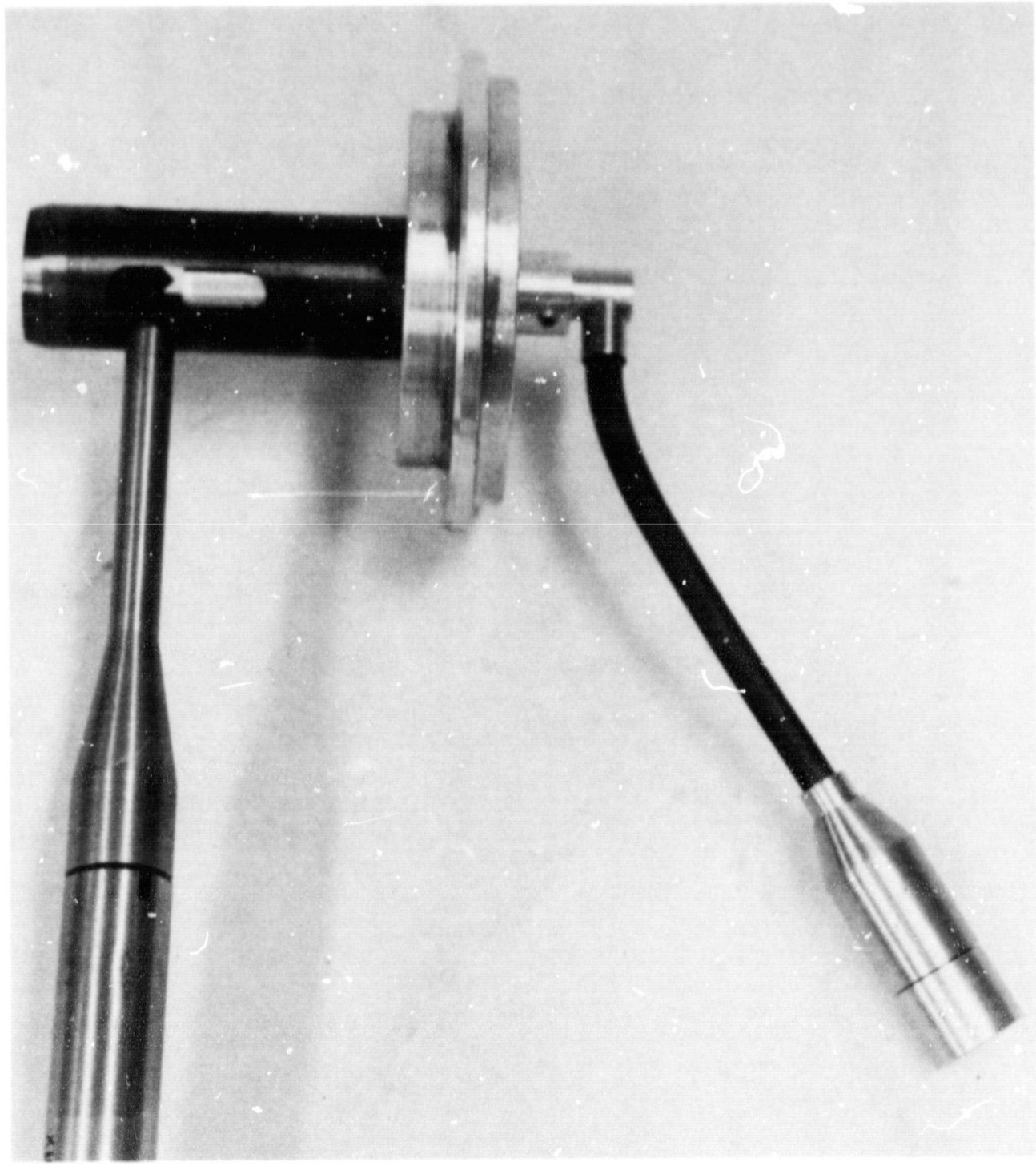

Figure 6. Pressure Transducer Location at the Base and the Mouth of the Resonance Tube

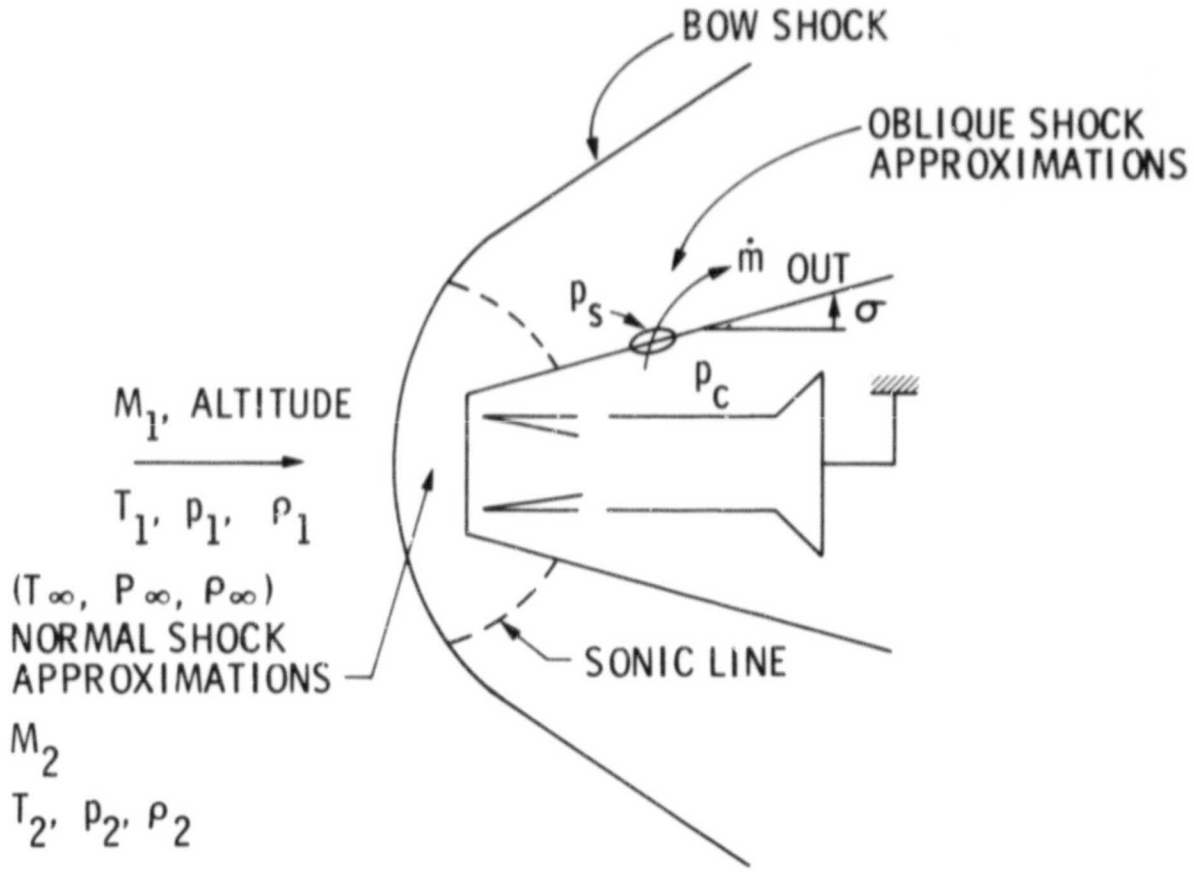

Figure 7. Calculation of Bench Flow Conditions

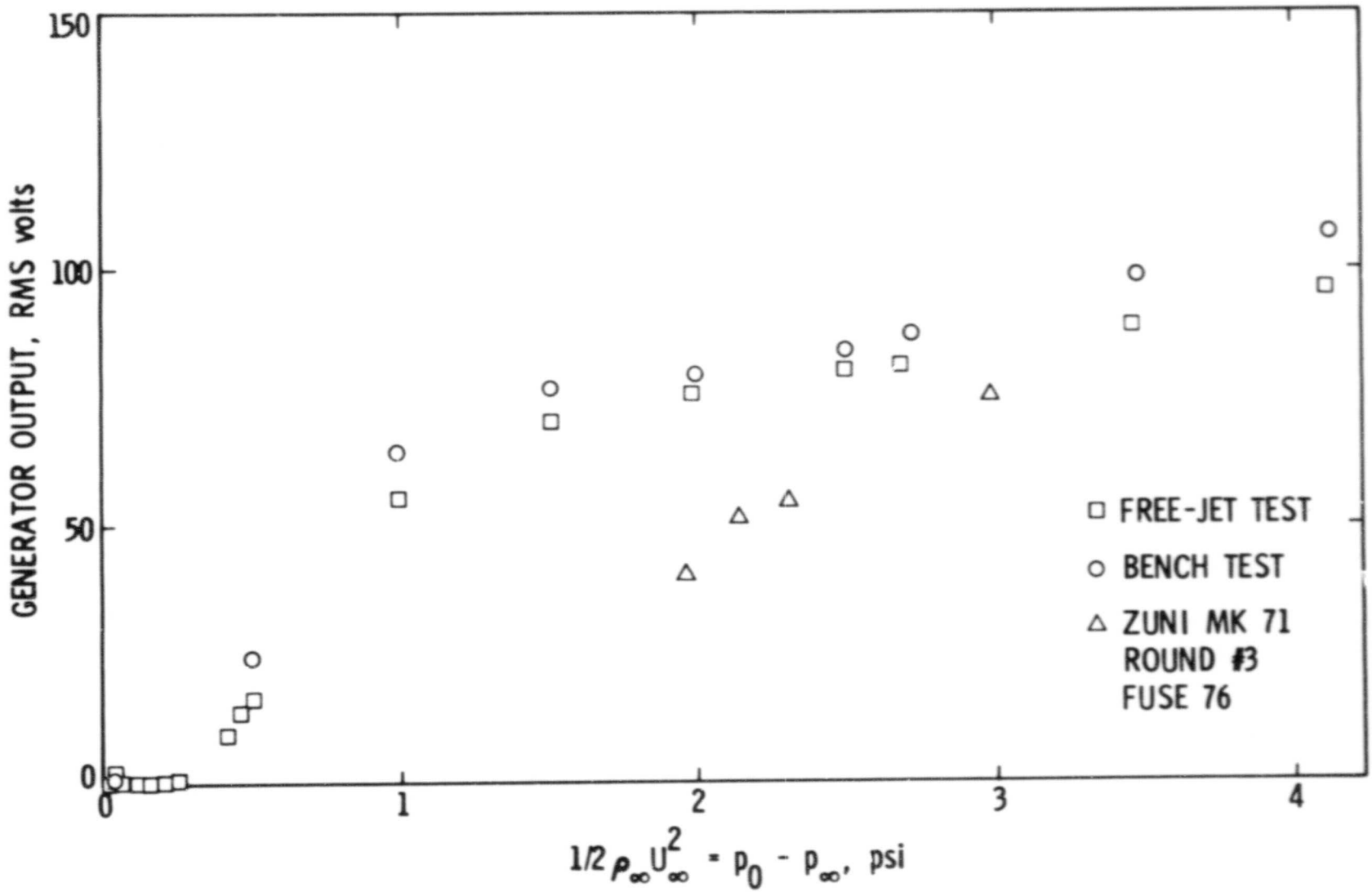

Figure 8. Comparison of Laboratory Measurements with Flight Data

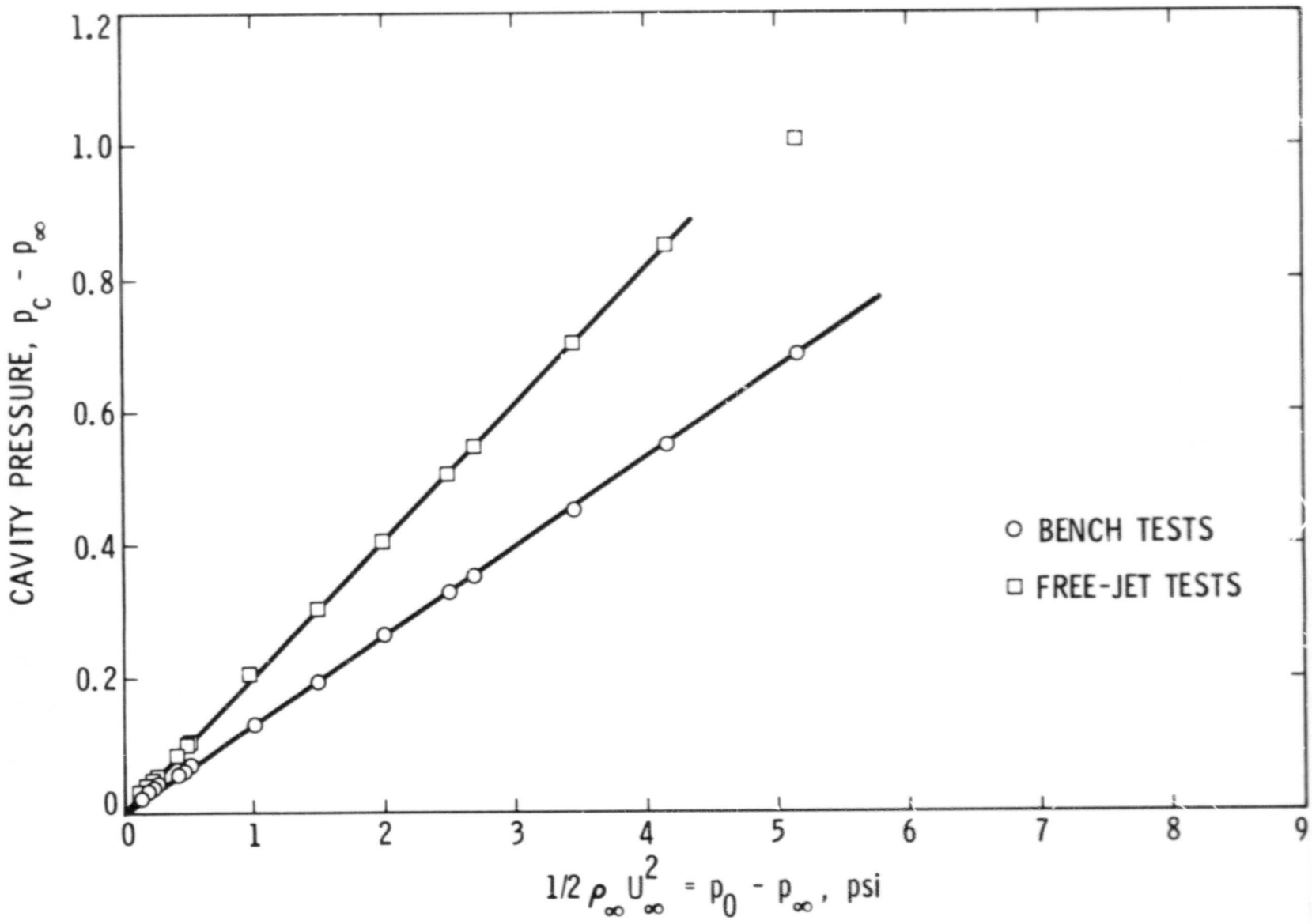

Figure 9. Cavity Pressure vs Free-Stream Dynamic Pressure

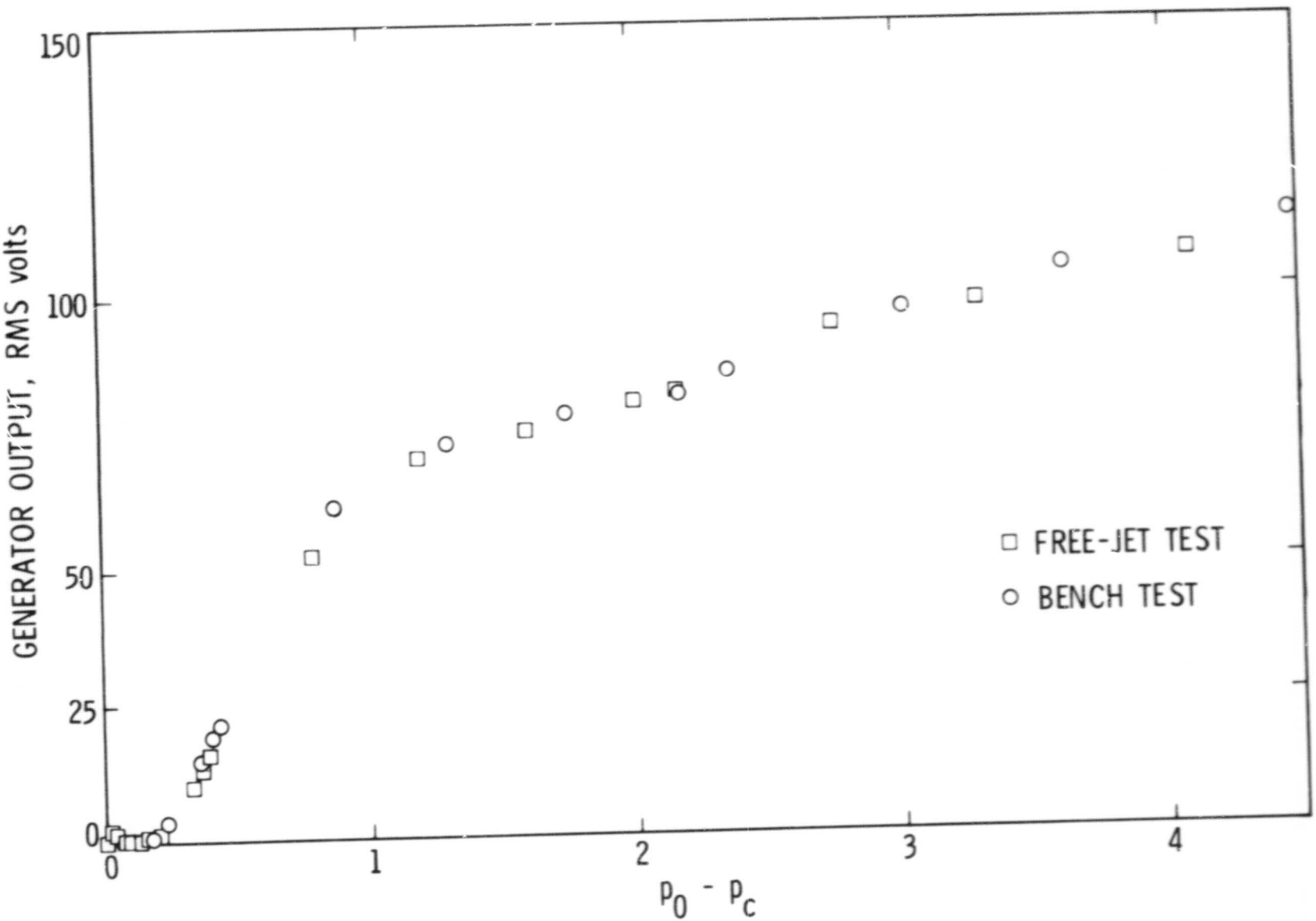

Figure 10. Comparison of Free-Jet Test Data with Bench Test Results

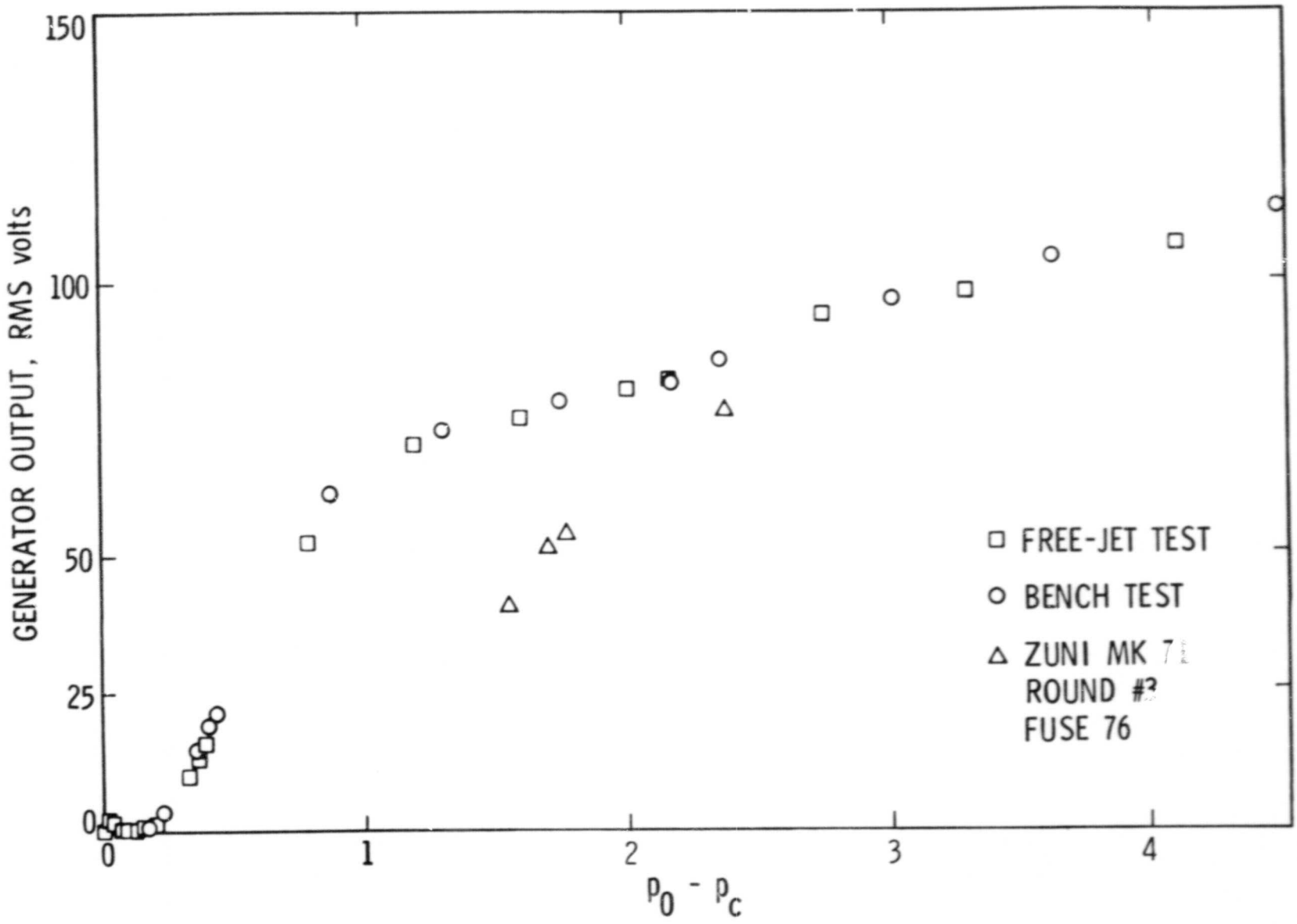

Figure 11. Comparison of Laboratory Measurements with Flight Data

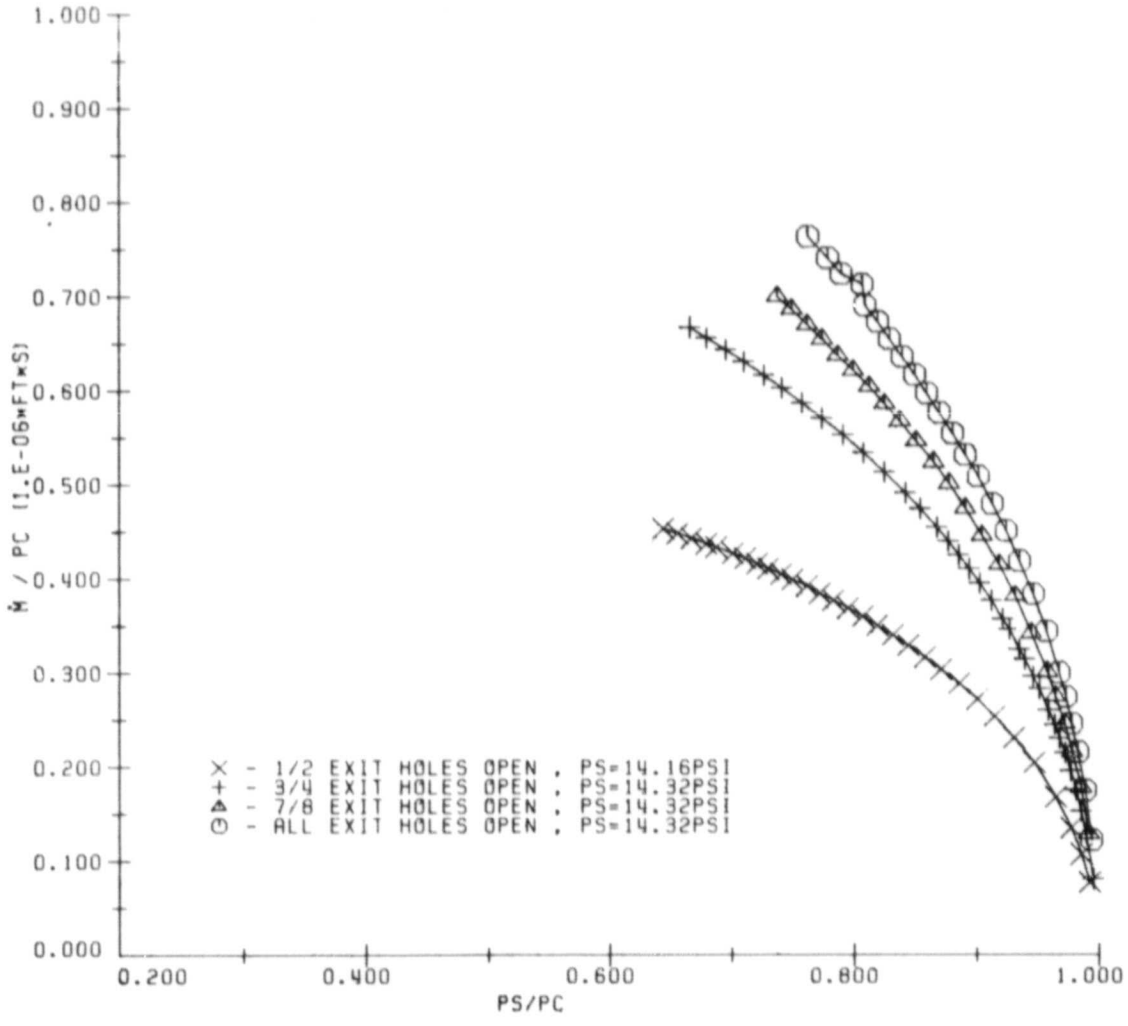

Figure 12. Mass Flow as a Function of P_s/P_c for Various Exit Areas

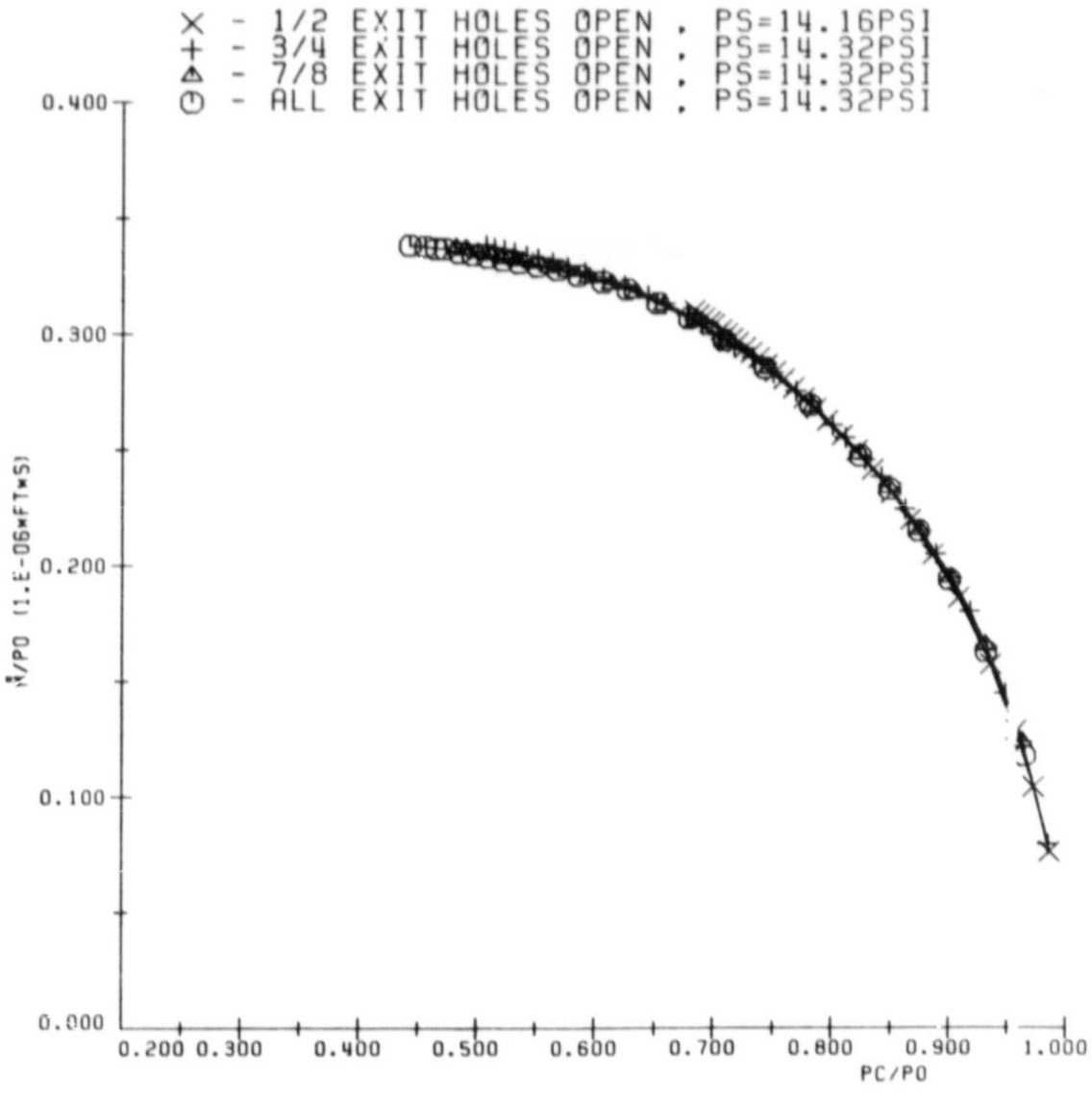

Figure 13. Mass Flow as a Function of P_c/P_0 for Various Exit Areas

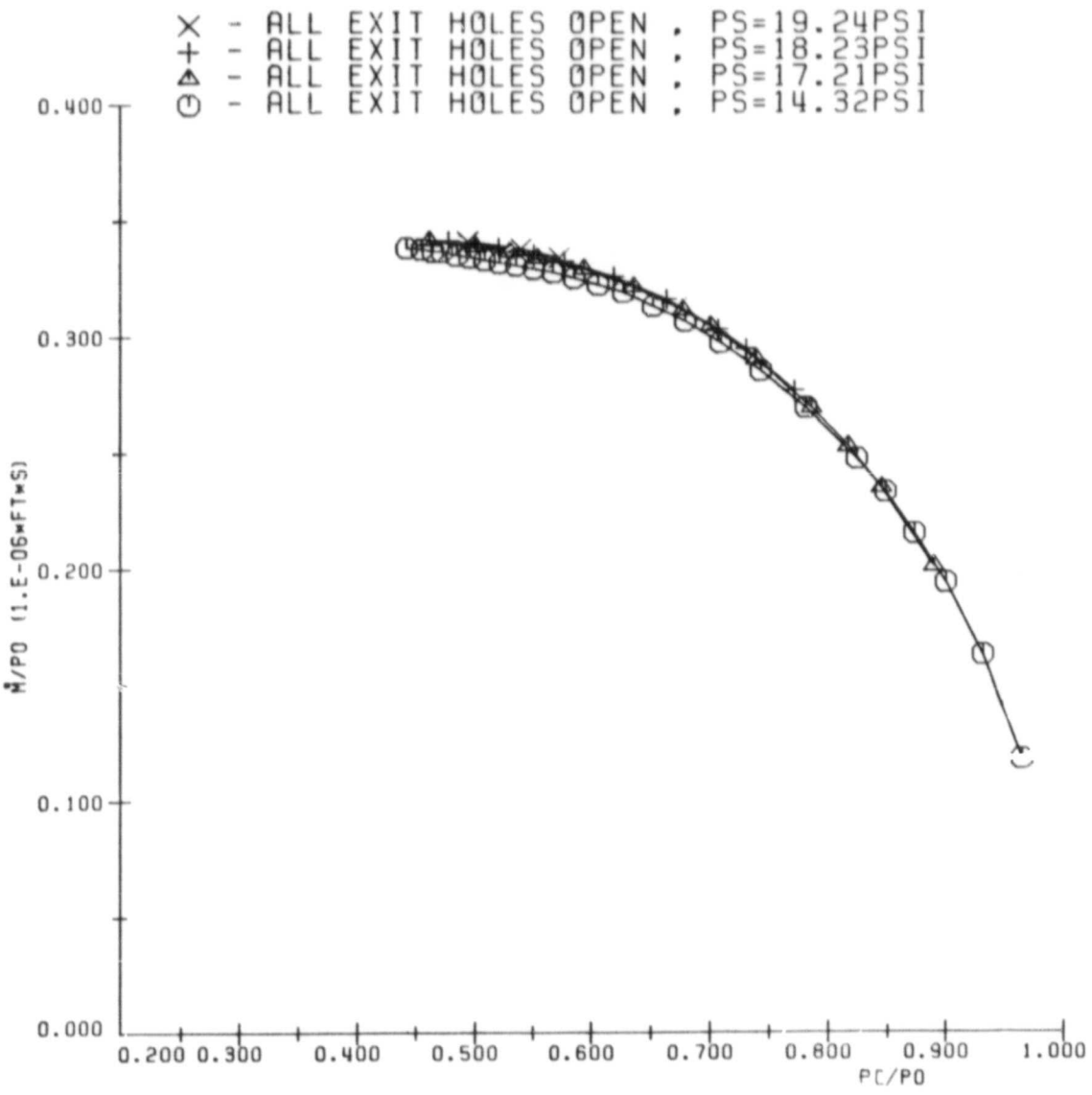

Figure 14. Mass Flow for Various Ambient Pressures

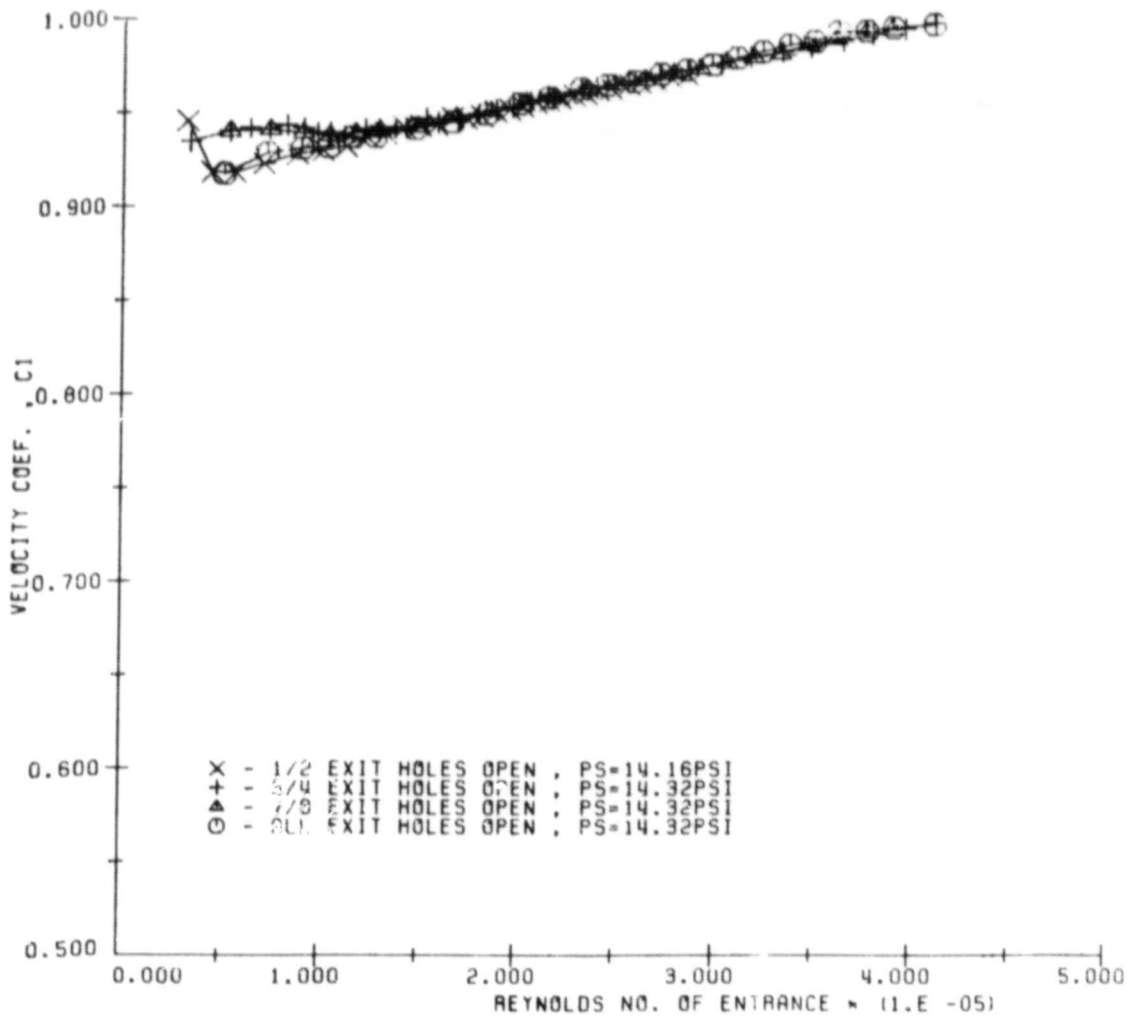

Figure 15. Velocity Coefficient vs Reynolds Number for Various Exit Areas

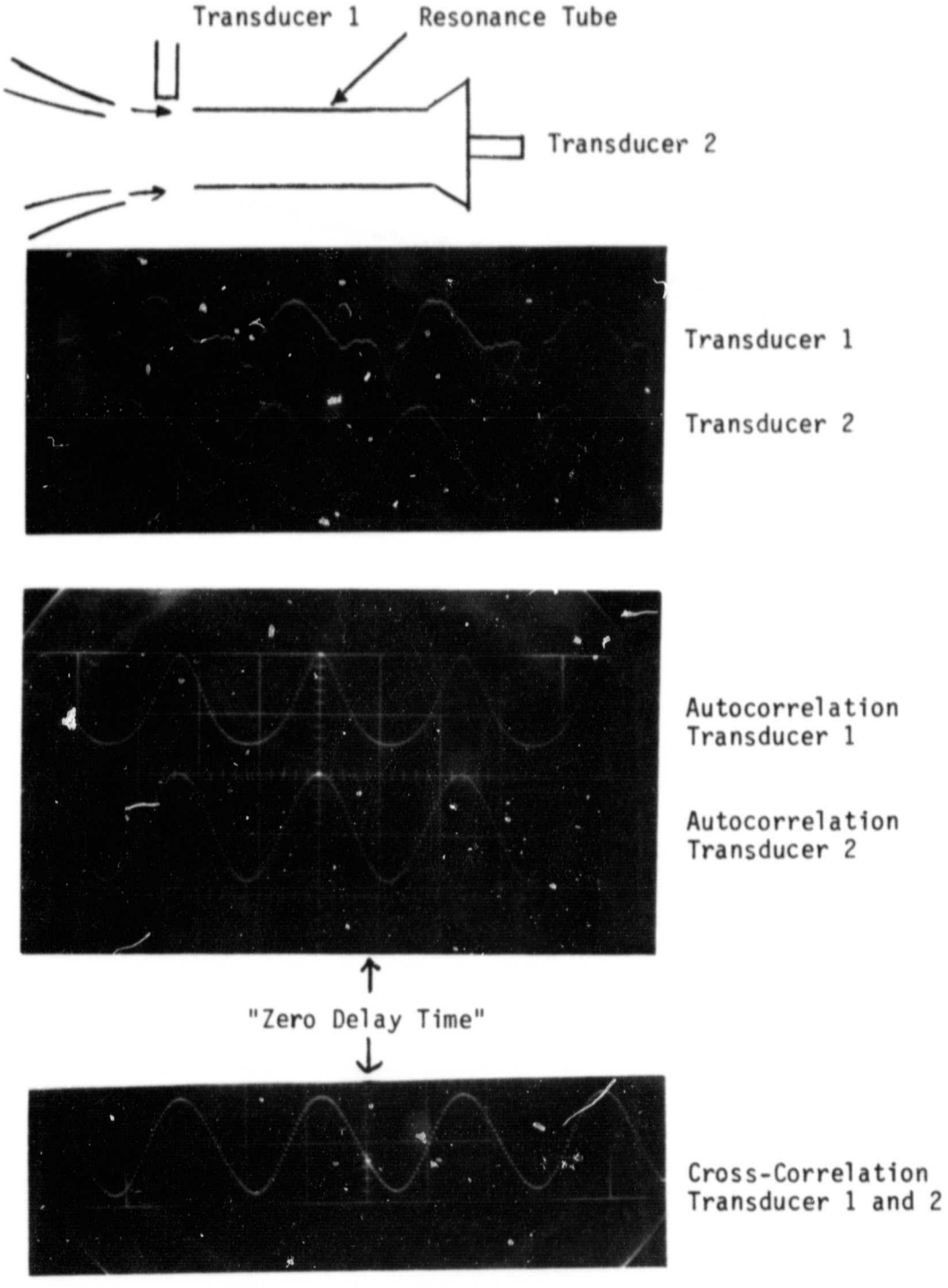

Figure 16. Pressure Transducer Output

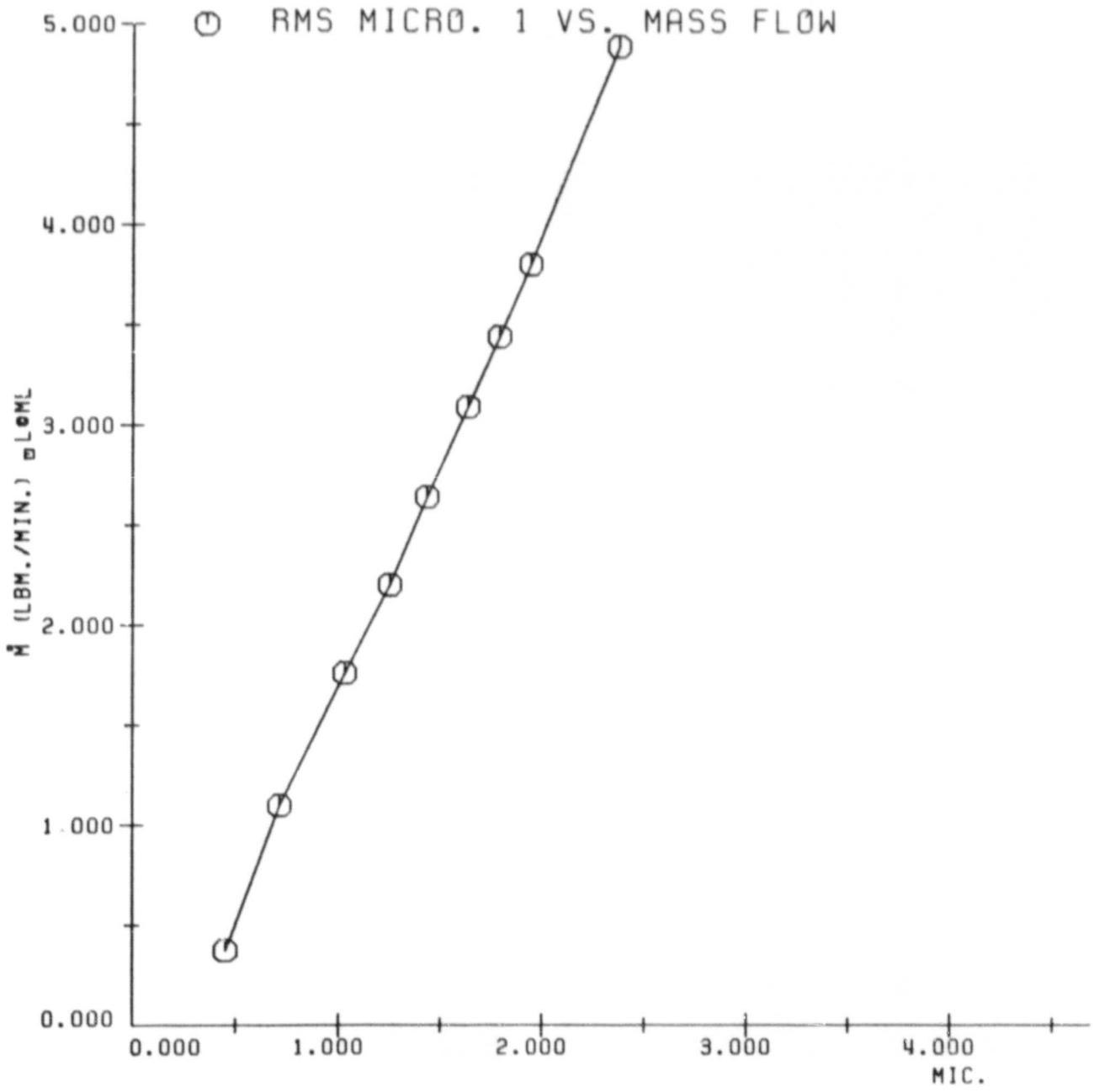

Figure 17. RMS Output of Pressure Transducer as a Function of Mass Flow Rate

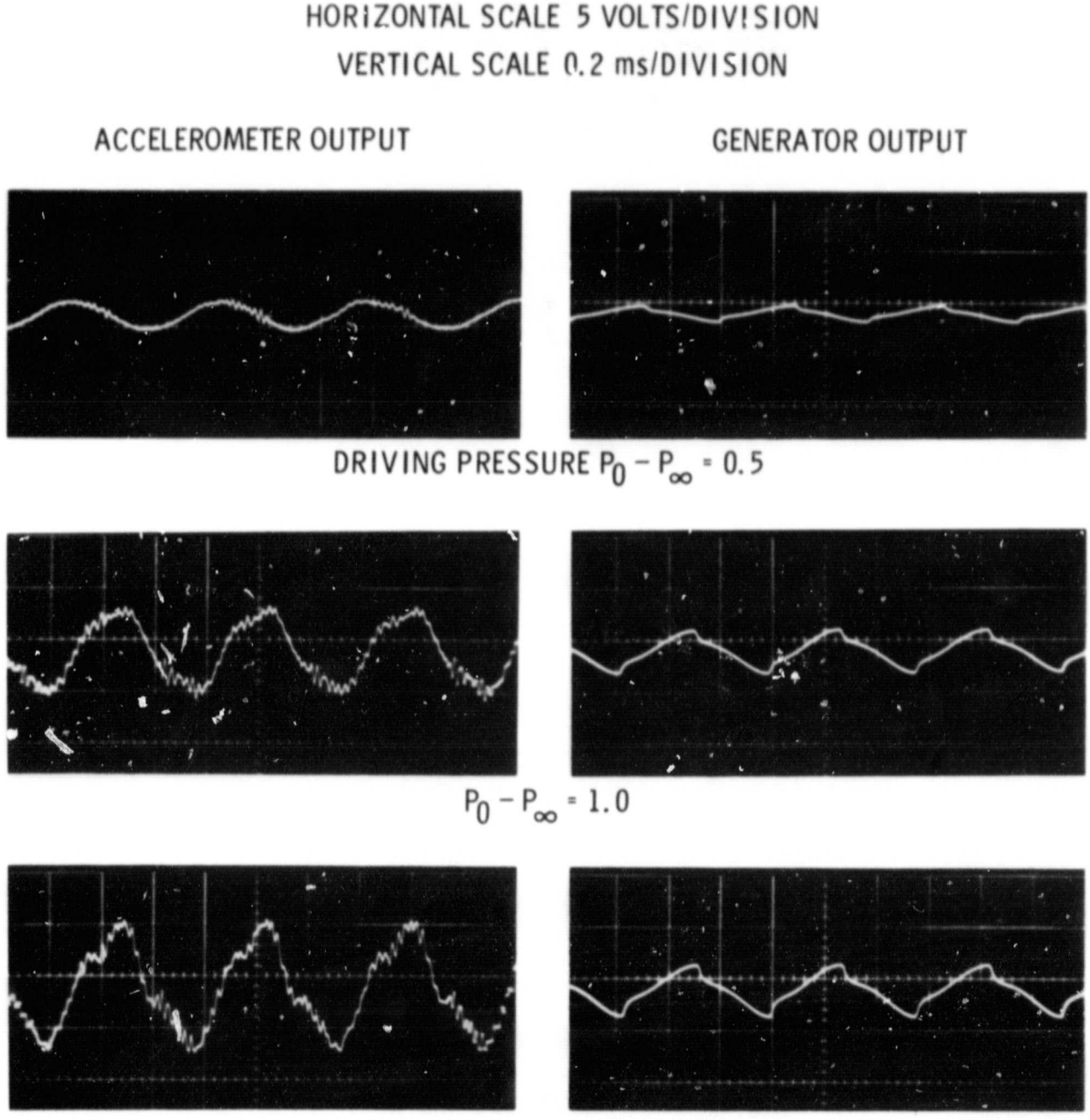

Figure 18. Oscilloscope Traces of Fluidic Generator

NATURAL FREQUENCY≒1412 Hz

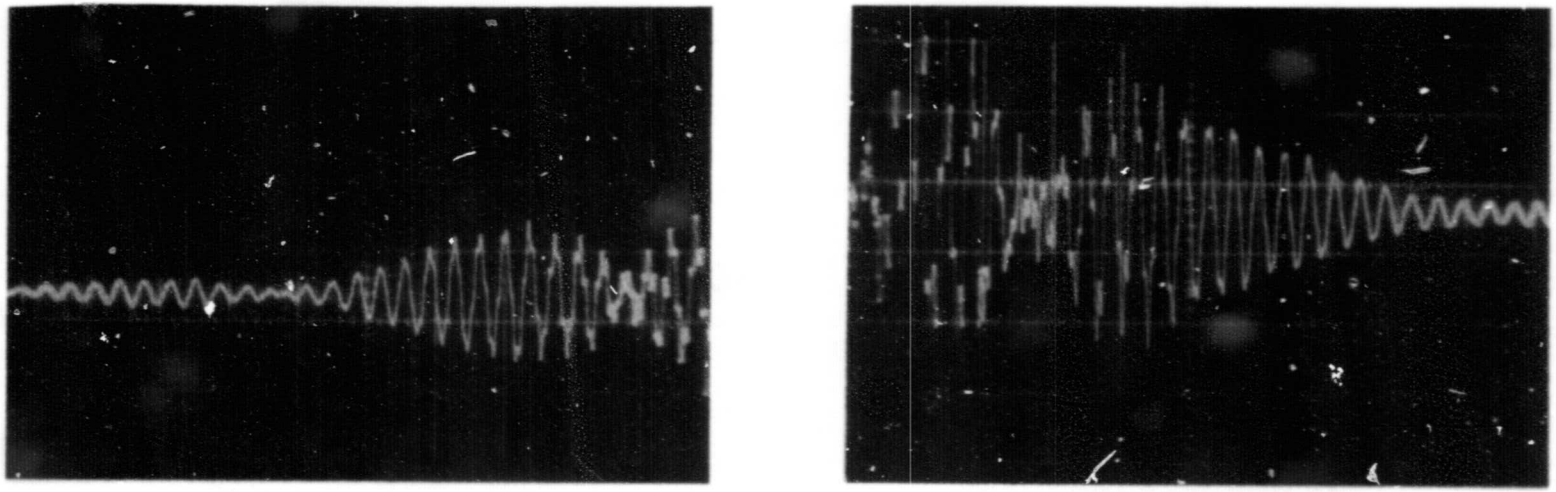

VERTICAL SCALE 0.05 VOLTS/DIVISION
HORIZONTAL SCALE 2 ms/DIVISION

Figure 19. Transient Response of Diaphragm-Reed Subsystem

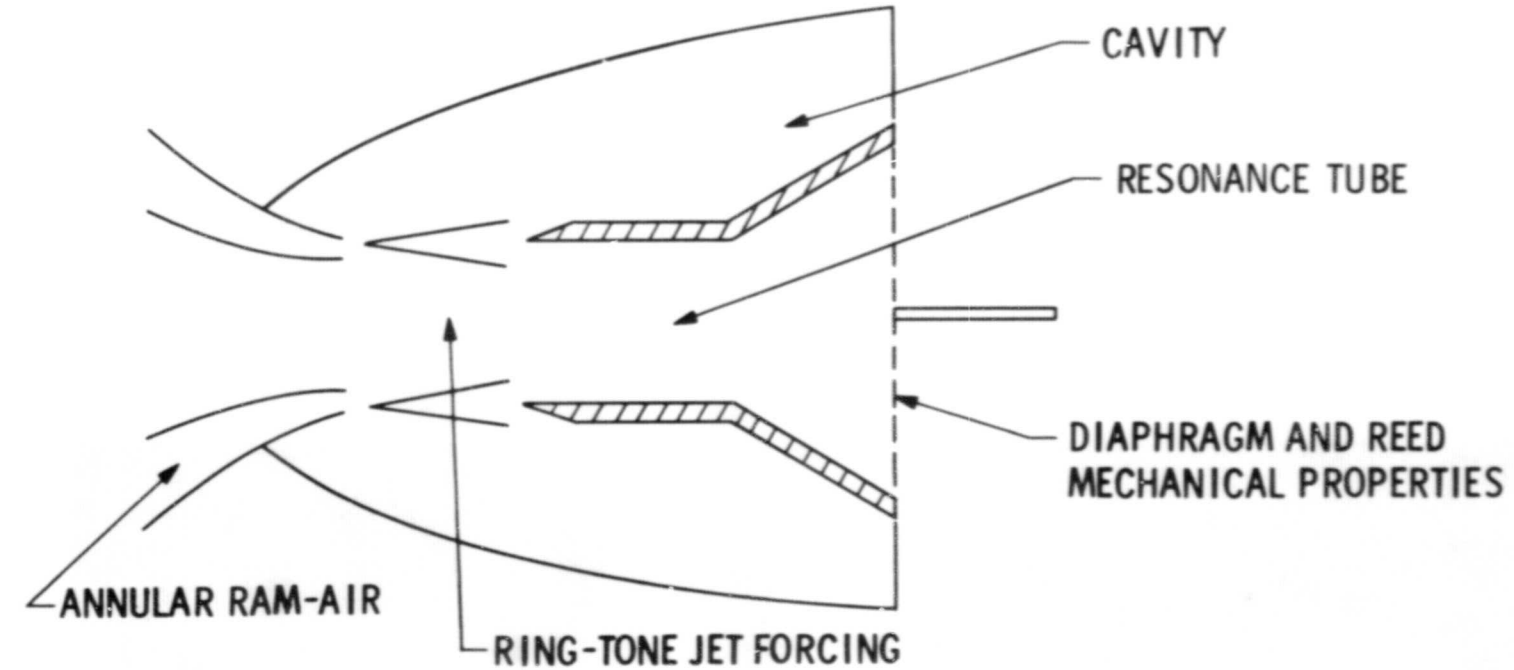

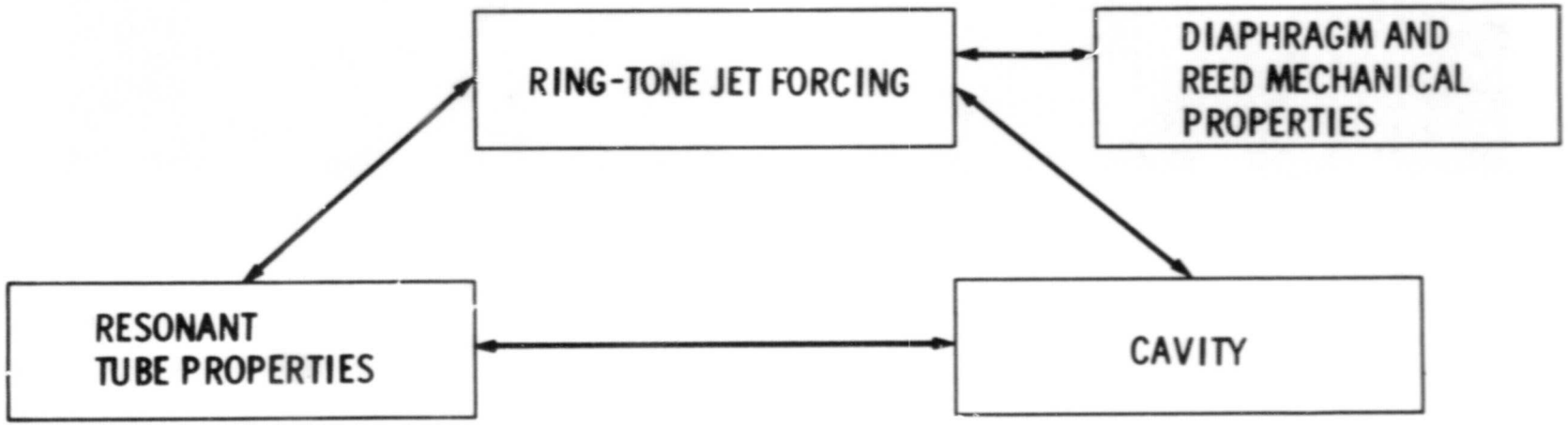

Figure 20. Modeling of Fluidic Electric Generator

NASA—JPL—Coml, LA, Calif